Electrostatic Interactions in Colloidal Suspensions: Tests of Pairwise Additivity

Eric S. Reiner and C. J. Radke
Dept. of Chemical Engineering, University of California, Berkeley, CA 94720

The electrical double-layer free energy is computed numerically for a model colloidal suspension of charged, hexagonally-packed monodisperse cylinders in a symmetric electrolyte solution using the Poisson-Boltzmann equations. Comparison is made to the energies estimated from sums of pair interactions and from two versions of a radially-symmetric cell model: one in which the outer boundary of the cylindrical cell is chosen to make the particle volume fraction Φ in the approximate model agree with that of the full lattice and the other in which the position of the outer boundary is chosen as half the nearest neighbor separation in the lattice. Calculations are performed for ranges of particle volume fractions from infinite dilution to 98% of closest packing, ionic strengths (in terms of the ratio of Debye length to particle radius λ/a) from 0.1 to 10.0, and dimensionless surface potentials and charge densities from 0.1 to 10.0.

The pair approximation is valid only when typical interparticle spacings are greater than the Debye length. The first implementation of the cell model proves quite accurate, while the second is only qualitatively correct. The magnitude of particle surface charge density or potential has little effect on these conclusions.

Introduction

Concentrated suspensions of particulates are of considerable importance in a number of current and emerging technological processes. Paints and inks are produced by dispersing finely-divided pigment in an aqueous or hydrocarbon solvent. A promising approach to the production of high-strength ceramic materials involves the processing of very concentrated (volume fraction of solids $\Phi > 30$–40%), nonaggregating dispersions of colloidal ceramic powders (Barringer and Bowen, 1983).

In recent years, much attention has been devoted to experimental characterization and theoretical prediction of the structural and rheological properties of concentrated suspensions. Monodisperse, submicron-sized polystyrene spheres have been observed to order into periodic structures which resemble atomic crystals (Luck et al., 1963; Hiltner and Krieger, 1969; Barclay et al., 1972; Wadati and Toda, 1972; Hachisu et al., 1973; Kose et al., 1973; Hachisu and Kobayashi, 1974; Kose and Hachisu, 1974; Takano and Hachisu, 1977, 1978a, b; Hachisu and Yoshimura, 1980; Williams and Crandall, 1974; Williams et al., 1976). Hexagonally-ordered structures have been observed in suspensions of tobacco mosaic virus (TMV) (Bernal and Fankuchen, 1941; Millman et al., 1984); liquid crystal phases of rod-like micelles (Parsegian, 1966; Winsor, 1968; Wennerström and Lindman, 1979; Tiddy, 1980); and solutions of DNA (Rau et al., 1984; Brandes and Kearns, 1986; Guldbrand et al., 1986), muscle fibers (Elliott, 1968; Millman and Nickel, 1980), and other biological materials. Laser light diffraction experiments also suggest a variety of structural effects in sheared systems (Hoffman, 1972, 1974, 1982; Clark and Ackerson, 1980; Ackerson and Clark, 1981, 1984; Ackerson and Pusey, 1988). Simulations and perturbation theories have succeeded in reproducing the "freezing" transition of suspensions of spherical particles with nearly quantitative accuracy (Snook and van Megen, 1976; van Megen and Snook, 1976a, b, 1978), and much effort is currently being directed toward the prediction of transport behavior (Bossis and Brady, 1984; Bagchi and Thirumalai, 1988).

Prediction of the structural and rheological properties of colloidal dispersions requires accurate information about particle interactions. Two of the most important of these are the attractive van der Waals and the repulsive electrostatic potentials. A plot of these interactions vs. surface-surface separation h for an isolated pair of particles is shown in Figure 1. The van der Waals potential V_a derives from the molecular dispersion (London) forces between the atoms within each par-

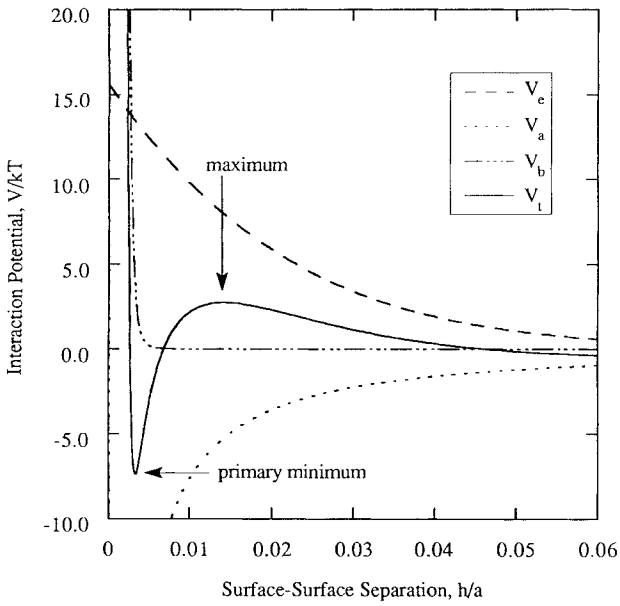

Figure 1. Representative colloidal interaction potentials vs. surface-surface separation *h/a*.

Addition of electrostatic (V_e), van der Waals (V_a), and short-range repulsive potentials may produce a strongly attractive primary minimum in the total potential (V_t), promoting aggregation. This process is inhibited by the maximum in V_t.

ticle. This potential is usually strongly attractive and encourages the particles to agglomerate. The electrostatic interaction V_e arises because of the dissociation of ionic groups on the particle surfaces or the adsorption of ions from the solvent. Its magnitude depends on the particles' surface charges and the ionic strength and dielectric properties of the solvent. As the concentration of ions (present to some extent in most polar solvents) increases, the repulsion is screened and is, therefore, less effective in keeping the particles apart. This interaction decays exponentially as h/λ, where λ, the screening or Debye length, is a characteristic measure of the extent of the electrical double layer and is inversely proportional to the square root of the ionic strength of the solvent. At separations h of a few Ångstroms or less, the repulsion V_b between the electrons of the individual atoms at the particles' surfaces dominates their interaction.

The balance between these interactions determines the phase behavior of a suspension. In the figure, the sum $V_t = V_a + V_e + V_b$ possesses a strong attractive minimum, which leads to instability to agglomeration. This process is retarded by the repulsive maximum. In concentrated suspensions, aggregation of many particles forms a disordered floc phase. Conversely, if V_e is large and long-ranged, or if the dispersion is so concentrated that interactions between neighboring particles are strongly repulsive, the suspension will tend to form an ordered lattice to minimize its potential energy.

It is important to understand how, if at all, interparticle potentials are altered in the concentrated systems that are of practical interest. The van der Waals attraction is usually calculated by integrating the attractive r^{-6} London pair potential over the interiors of a pair of particles (Hamaker, 1937). While this procedure is not rigorous, London forces are well approximated as pairwise additive. In contrast, the electrostatic interaction is calculated by solving a mean-field theory for the ion distributions in the solvent surrounding the particles (Levine, 1934, 1939a, b, c). Most theoretical studies to date have estimated this interaction by summing pair potentials obtained from approximate solutions to the linearized Poisson-Boltzmann (or Debye-Hückel) equation for two spheres. These include the lubrication approximation of Derjaguin (Derjaguin, 1934, 1939; Derjaguin and Landau, 1941) and its extensions (Hogg et al., 1966; McCartney and Levine, 1969; Bell et al., 1970; Honig and Mul, 1971; Bell and Peterson, 1972; Usui, 1973; Kar et al., 1973; Ohshima et al., 1982, 1983), and the weak overlap approximation of Levine (1934, 1939c; Verwey and Overbeek, 1948; Bell et al., 1970). These have been extensively compared to perturbative and numerical solutions of the linear (hereafter denoted by DH) and full nonlinear (PB) equations (Levine, 1939b,c; Hoskin and Levine, 1956; McCartney and Levine, 1969; Bell et al., 1970; Glendinning and Russel, 1983), and accurate expressions for pair interactions for a wide variety of conditions are available (Bell et al., 1970; Honig and Mul, 1971; Ohshima et al., 1982, 1983).

While these approximations are excellent in dilute suspensions, two phenomena characteristic of concentrated systems may lead to errors. First, isolated pairs are rare, and each particle's double layer overlaps that of several others, causing the interaction energy to depend on the configuration of many particles. Second, the entire volume of electrolyte interacts with the suspended material. A basic assumption of the PB and DH theories is that interacting particles are surrounded by a "bulk" region of fluid that acts as a source or sink for ions. In a concentrated suspension this is no longer the case, and the screening of repulsion between charged surfaces is affected (Bell and Levine, 1957; Chen and Levine, 1972).

Several researchers (Fuoss et al., 1951; Alfrey et al., 1951; Marčelja et al., 1976) have proposed a cell model that attempts to account for these effects. In this approach, the often complicated distribution of neighbors surrounding a particle is replaced by imagining that each particle in a concentrated suspension is effectively isolated within a simplified (cylindrical or spherical) cell. The outer cell boundary is normally chosen to result in the desired volume fraction. An alternative choice for the location of this surface is one-half of the mean nearest neighbor separation. This option is appropriate for conditions approaching closest packing where forces between nearly touching surfaces might be expected to dominate. These models do not reproduce the detailed geometrical effects of interacting particle surfaces, but have been used to make qualitative predictions of ordering (Marčelja et al., 1976; Beunen and White, 1981; Ohtsuki et al., 1981; Shih and Stroud, 1983) and have also been used to correct partially for fixed ionic concentrations (Alexandrowicz, 1962; Alexandrowicz and Katchalsky, 1963; Beunen and White, 1981; Shih and Stroud, 1983).

The objective of this work is to perform a critical quantitative study of the effect of the first of these phenomena (multiple double-layer overlap) on the accuracy of the pairwise additivity and symmetric cell approximations. A two-dimensional model is adopted of regular, hexagonally-packed cylinders with fixed surface charges or potentials immersed in an ionic solution characterized by its Debye length. This model permits the impact of multiparticle geometry in concentrated dispersions to be evaluated rigorously. The nonlinear Poisson-Boltzmann equation and its linearized form, the Debye-Hückel equation, which relate the ion distributions near the colloid surfaces to

the electrostatic potential, are solved using a variational finite element method, which leads directly to the calculation of the configurational free energy. The hexagonal lattice results are compared to those obtained by solving the same equations for isolated pairs of particles and summing the resulting pair potentials and by computing the configurational free energies of the radially-symmetric cell model with both choices for the location of the outer boundary. The effects of varying the particle concentration, uniform surface charge and potential, and solvent ionic strength (via the Debye length) are examined.

Electrostatic Interactions in Concentrated Suspensions

To calculate the electrostatic interaction energy W_e of a configuration of colloidal particles, it is necessary to predict the distribution of screening ions in the electrical double layer surrounding the particles and to relate that distribution to the electrostatic potential ψ. The potential at a point in space $\underline{r}$ is related to the charge distribution $\rho_e(\underline{r})$ through Poisson's equation:

$$\epsilon_0 \underline{\nabla} \cdot (D \underline{\nabla} \psi) = -\rho_e, \tag{1}$$

where D is the local value of the solvent's dielectric constant and ϵ_0 is the dielectric permittivity of free space. In an electrolyte solution containing n species of ions near a charged interface, ρ_e is simply the charge density due to the ion singlet distributions g_i:

$$\rho_e(\underline{r}) = \sum_{i=1}^{n} z_i e C_i^0 g_i(\underline{r}), \tag{2}$$

where e is the unit charge, and z_i and C_i^0 are the valence and bulk concentration of ion i; the latter may be defined as the concentration of i in an infinite reservoir of electrolyte in thermodynamic equilibrium with the interfacial region. The solvent is assumed to act as a continuum, entirely characterized by the local value of its dielectric constant D. The distribution functions $g_i(\underline{r})$ depend on the potential as well as on nonelectrostatic surface-ion and ion-ion interactions.

In the approximation of Guoy (1910) and Chapman (1913), ions are assumed to behave as point charges only. If such an ion is reversibly transferred from a reservoir at zero applied potential to a location within the double layer at potential ψ, the work done on the charge is $z_i e\psi$. This configuration of ion i is therefore weighted by the Boltzmann factor $\exp(-z_i e\psi/kT)$ relative to its initial position. Rigorously, g_i should be averaged over all possible numbers and configurations of ions. Usually, however, g_i is assumed to equal its mean-field value:

$$g_i(\underline{r}) = \exp(-z_i e\psi/kT). \tag{3}$$

This assumption ignores fluctuations in the potential, causing an error in g_i of order $\langle\psi^2\rangle - \langle\psi\rangle^2$, where the brackets represent averaging in the grand ensemble. The PB equation is obtained by combining Eqs. 1, 2 and 3 in a region of constant D:

$$\nabla^2\psi = \frac{-e}{D\epsilon_0} \sum_{i=1}^{n} z_i C_i^0 \exp(-z_i e\psi/kT). \tag{4}$$

At low potentials, where the mean-field approximation becomes rigorous, the exponential in Eq. 4 may be linearized. After elimination of constant terms that vanish because of bulk electroneutrality, the DH equation may be written as:

$$\nabla^2\psi = \frac{\psi}{D\epsilon_0 kT} \sum_{i=1}^{n} (z_i e)^2 C_i^0 = \lambda^{-2}\psi. \tag{5}$$

The Debye length, λ, is defined by Eq. 5. These approximations (Eqs. 4 and 5) have been subjected to extensive formal and computational tests (Fixman, 1979; Torrie and Valleau, 1980; van Megen and Snook, 1980; Snook and van Megen, 1981; Henderson and Blum, 1978, 1980, 1981; Henderson et al., 1979; Lozada-Cassou et al., 1982; Lozada-Cassou and Henderson, 1983; Blum et al., 1983; Carnie, et al., 1981; Carnie and Chan, 1982; Carnie et al., 1984; Carnie, 1985; Linse and Jönsson, 1983; Le Bret and Zimm, 1984; Bacquet and Rossky, 1984; Murthy et al., 1985; Mills et al., 1985; Vlachy and Haymet, 1986; Guldbrand et al., 1986). The PB equation describes the double layer well at small surface charges ($q_s < 0.1$ C/m^2) and low-bulk ionic strengths ($\lambda > 1$ nm). At higher charges and electrolyte concentrations, both equations fail to predict structural correlations near the interface. These deficiencies may be corrected partially by considering explicitly the formation of Stern layers near the surface.

The next step in calculating the electrostatic interaction energy W_e is to compute the electrostatic free energy Ω_e of the interface relative to that of an uncharged surface. A number of different procedures are available, but perhaps the most elegant of these utilizes the observation that the Euler-Lagrange equations, which are obtained by extremizing a model free energy over the space of distribution functions (or, equivalently in this case, over the space of potential functions), are the mean-field equations which correspond to that model. One may reverse this process via the calculus of variations (Levine, 1939c; Reiner, 1991; Reiner and Radke, 1990):

$$\Omega_e = \int_S d\underline{r}^s \omega_s(\underline{r}^s) - \int_V d\underline{r} \left\{ \frac{D\epsilon_0}{2} |\underline{\nabla}\psi|^2 + (\Pi_{osm} - \Pi_{osm}^0) \right\}. \tag{6}$$

ω_s is a surface free energy density, which depends on the choice of boundary conditions that relate the surface charge q_s and potential ψ_s. When the surface potential is fixed ω_s vanishes, while at constant charge, $\omega_s = q_s\psi_s$. The regions of integration S and V are all charged boundaries and the entire interfacial region including the interiors of any solids, respectively. The $|\underline{\nabla}\psi|^2$ term is the Maxwell stress contribution to the energy of an electric field, while $(\Pi_{osm} - \Pi_{osm}^0)$ represents the excess osmotic pressure due to the net accumulation of ions in the double layer and is equal to:

$$kT \sum_{i=1}^{n} C_i^0 \{\exp(-z_i e\psi/kT) - 1\} \tag{7}$$

in the PB model and

$$D\epsilon_0 \lambda^{-2}\psi^2/2 \tag{8}$$

in the DH approximation. The Maxwell stress and osmotic pressure terms are usually neglected within the particle interiors, restricting the region of integration in Eq. 6 to the double layer surrounding the particles.

The configurational free energy W_e of a colloidal assemblage may be defined as the reversible work expended in a process whereby the particles are brought together from an (effectively) infinite separation to their final configuration at constant temperature T, system volume V, particle surface area S, and ionic chemical potentials μ_i or numbers N_i. Since we have fixed the bulk concentrations C_i^0 of the ions, we have specified their chemical potentials; the configurational free energy is, therefore, a grand canonical potential and may be obtained as the difference between the electrostatic free energies of the assemblage and the free energies of the individual particles isolated in the electrolyte. The electrostatic pair potential V_e between two isolated axisymmetric particles whose centers are separated by a distance d may be defined as:

$$V_e(d) \equiv W_e^{\text{pair}}(d) = \Omega_e^{\text{pair}}(d) - \Omega_e^{\text{pair}}(\infty). \tag{9}$$

For an arbitrary configuration of m particles (defined by the set of surface coordinates $\{\underline{r}_\nu^s;\ \nu = 1, \ldots, m\}$) immersed in an unbounded electrolyte, the pairwise additivity approximation may be expressed succinctly as:

$$\begin{aligned} W_e(\{\underline{r}_\nu^s; l = 1, \ldots, m\}) &\equiv \Omega_e(\{\underline{r}_\nu^s; l = 1, \ldots, m\}) - \Omega_e(\{\underline{r}_\nu^{s,\infty}; l = 1, \ldots, m\}) \\ &= \Omega_e(\{\underline{r}_\nu^s; l = 1, \ldots, m\}) - \sum_{l=1}^{m} \Omega_e(\{\underline{r}_\nu^{s,\infty}\}) \\ &\cong \sum_{\nu=1}^{m} \sum_{\nu'>\nu} [\Omega_e(\{\underline{r}_\nu^s, \underline{r}_{\nu'}^s\}) - \Omega_e(\{\underline{r}_\nu^{s,\infty}\}) - \Omega_e(\{\underline{r}_{\nu'}^{s,\infty}\})] \\ &= \sum_{\nu=1}^{m} \sum_{\nu'>\nu} V_e(\{\underline{r}_\nu^s, \underline{r}_{\nu'}^s\}), \end{aligned} \tag{10}$$

where $\underline{r}_\nu^{s,\infty}$ represents particle ν isolated in the electrolyte. Throughout this article, we implicitly calculate Ω_e and W_e with respect to a reference state of uncharged particle surfaces immersed in a homogeneous electrolyte (at zero electrostatic potential); this choice of reference states allows us to isolate the electrostatic component of particle interactions in W_e.

To complete the model, particle geometries and surface charge conditions must be chosen that permit critical testing of the pairwise additivity approximation. Such a choice should both correspond to a physically realistic system and lend itself to tractable computation. An ideal selection is an ordered array of monodisperse axisymmetric particles with fixed surface charges or potentials. This model represents the minimum energy state of a colloidal crystal. It allows the issue of multiparticle interactions to be addressed directly, while the presence of a high degree of symmetry minimizes the amount of computation required by limiting the region over which the potential must be approximated.

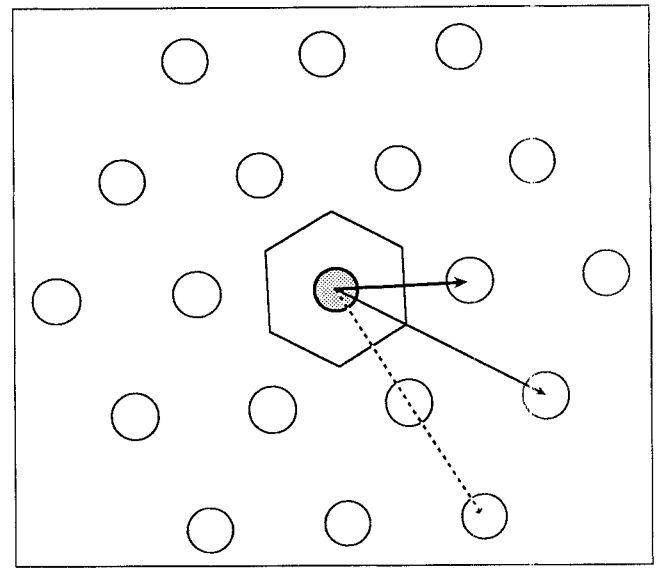

Figure 2. Portion of a hexagonal lattice.

The central particle is shaded (●); periodicity of the lattice limits the calculation to the region within the hexagonal cell. Neighbors are indicated by→ (nearest), – (second nearest), and -- (third nearest).

Model Description

We study a two-dimensional realization of this system, an infinite collection of cylinders (or disks) packed into a regular hexagonal array as shown in Figure 2. This geometry permits the achievement of close packing without the necessity of modeling the more complicated face-centered cubic or hexagonal close-packed structures in three dimensions. The model is also directly applicable to the micellar liquid crystals, DNA solutions, and TMV gels discussed in the introduction section.

The pairwise configurational energy per particle of a regular lattice may be reduced to a sum of pair interactions over shells of neighbors (Figure 2):

$$W_e^{\text{pair sum}} = 1/2 \sum_{\tau} Z_\tau V_e(d_\tau). \tag{11}$$

d_τ is the distance between the centers of a chosen particle and its neighbors in shell τ, and Z_τ is the coordination number of that shell. For a hexagonal array, the first 11 of these values are shown in Table 1.

Table 1. Hexagonal Array: Shell Distances and Coordination Numbers

Shell No., τ	Center-Center Distance, d_τ/d_1	Coordination No., Z_τ
1	1.0000	6
2	1.7321	6
3	2.0000	6
4	2.6458	12
5	3.0000	6
6	3.4641	6
7	3.6056	12
8	4.0000	6
9	4.3589	12
10	4.5826	12
11	5.0000	6

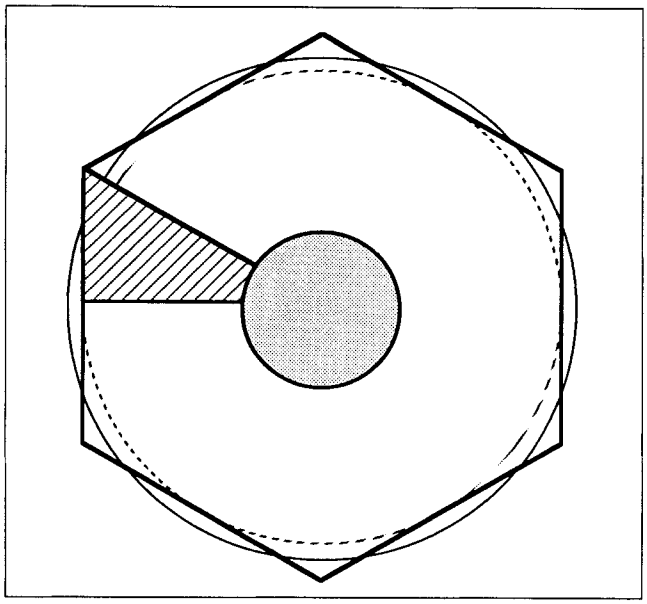

Figure 3. Closeup of hexagonal cell.

Symmetry of the cell permits consideration of only the hatched (□) subcell. Boundaries of the approximating cylindrical (radially symmetric) models are shown, as ——— (volume-equivalent) and — — — (nearest surface).

The exact value of Ω_e per particle is simply the integral of ω_s over a particle surface minus the Maxwell stress and osmotic pressure densities (cf. Eq. 6) integrated over the hexagonal cell (shown in Figure 2) that surrounds the particle. As shown in Figure 3, the cell possesses sixfold rotational symmetry and an additional mirror symmetry across any line that passes through the particle center and bisects one side of the hexagon. Hence, only one twelfth of the cell need be considered:

$$W_e^{\text{particle}} = 12 W_e^{\text{subcell}} \tag{12}$$

It is important to choose physically meaningful conditions at the particle surface. The most commonly studied condition is that of constant potential ψ_s. This assumption may be appropriate for metal sols in a solution where the metal is present in ionic form, and the surface charge is established by the adsorption of these ions onto the particle surfaces. If the surface charge is induced by the dissociation of ionogenic groups at the particle/solution interface, as is true for biomaterials and the metal oxides which are of interest in paint and ceramics applications, a more appropriate choice of boundary conditions is that of constant charge density q_s. In this case, the charge per unit area is determined by the number of dissociated groups at the particle surface. In such systems the potential is actually regulated by the dissociation mechanism as the particles are moved together, so that the boundary condition varies between the constant potential and constant charge extremes (Bierman, 1955a,b; Ninham and Parsegian, 1971; Brenner and McQuarrie, 1973a,b,c; Chan et al., 1975, 1976; Healy et al., 1980). Consideration of such mechanisms requires the specification of additional parameters (e.g., dissociation constants). Since our goal was to study the fundamental validity of the pairwise additivity and symmetric cell approximations, we chose to consider only the two idealized models. Our calculation may be extended readily to models for charge regulation (Reiner, 1991).

In all of the calculations discussed below, a 1-1 (e.g., alkali halide) electrolyte is considered. While this particular choice is immaterial in the DH approximation since the properties of the electrolyte appear only in the screening length λ, it does permit simplification of the PB equation. If the potential ψ is scaled by e/kT,

$$\nabla^2\psi^* = \frac{2e^2C_1^0}{D\epsilon_0 kT}\sinh(\psi^*) = \lambda^{-2}\sinh(\psi^*) \tag{13}$$

is obtained. The remaining parameters in the model are the surface charge density q_s or surface potential ψ_s, the particle radius a, and the nearest-neighbor separation d_1 or volume fraction Φ, which are related by:

$$\Phi = \frac{2\pi}{\sqrt{3}}\left(\frac{a}{d_1}\right)^2. \tag{14}$$

Because our model is strictly two-dimensional, it is more precise to consider Φ an *area* fraction. However, since the interactions we calculate are applicable to physical systems of elongated cylinders, little rigor is lost in treating Φ as a volume fraction.

All lengths may be scaled by the particle radius:

$$\lambda^* = \lambda/a;\ d_1^* = d_1/a;\ \underset{\sim}{\nabla}^* = a\underset{\sim}{\nabla}. \tag{15}$$

The surface charge density or surface potential and free energies may be scaled similarly:

$$q_s^* = \frac{q_s ea}{D\epsilon_0 kT} = -\underset{\sim}{\nabla}^*\psi^* \cdot \underset{\sim}{n}\,|_{\underset{\sim}{r}^s};\ \psi_s^* = \frac{e\psi_s}{kT}; \tag{16}$$

$$\Omega_e^* = \frac{\Omega_e}{D\epsilon_0}\left(\frac{e}{kT}\right)^2;\ W_e^* = \frac{W_e}{D\epsilon_0}\left(\frac{e}{kT}\right)^2. \tag{17}$$

It is important to note that in three dimensions, W_e and Ω_e are free energies per length of cylinder a.

In both the isolated pair and hexagonal geometries, it is convenient to make a change from Cartesian coordinates $z = x + iy$ to bipolar coordinates $z' = \xi + i\eta$. If the x axis is chosen as the line passing through the centers of two particles and the origin is fixed at the midpoint of the segment joining these points, the transformation may be defined by (Happel and Brenner, 1973; Morse and Feshbach, 1953):

$$z = ib\cot(z'/2), \tag{18}$$

or

$$x = \frac{b\sinh(\eta)}{\cosh(\eta) - \cos(\xi)};\ y = \frac{b\sin(\xi)}{\cosh(\eta) - \cos(\xi)}. \tag{19}$$

Curves of constant η $(-\infty < \eta < \infty)$ are circles of radius $b\,|csch(\eta)|$ centered at $[x = b\coth(\eta), y = 0]$. Curves of constant ξ $(0 \le \xi < 2\pi)$ are circular arcs of radius $b\,|csc(\xi)|$ and center $[x = 0, y = b\cot(\xi)]$. The surfaces of an identical pair of particles of radius a separated by distance d_1 become the pair of lines $\eta = \pm\eta_0 = \pm\cosh^{-1}(d_1^*/2)$. The parameter b may also be scaled with the particle radius and takes the value:

$$b^* = b/a = \sqrt{(d_1^*/2)^2 - 1}. \tag{20}$$

From Eq. 6, the dimensionless free energy functional per particle becomes:

$$\Omega_e^* = 2N_c b^* \int_{\xi_0(\eta_0)}^{\pi} \frac{d\xi \omega_s^*(\xi)}{d_1^*/2 - \cos(\xi)} - 2N_c \int_0^{\eta_0} d\eta \int_{\xi_0(\eta)}^{\pi} d\xi \left\{ \frac{1}{2}\left[\left(\frac{\partial \psi^*}{\partial \xi}\right)^2 + \left(\frac{\partial \psi^*}{\partial \eta}\right)^2 \right] + \left(\frac{b^*}{\cosh(\eta) - \cos(\xi)}\right)^2 (\Pi_{osm}^* - \Pi_{osm}^{*0}) \right\}, \tag{21}$$

where ω_s^* equals $q_s^* \psi_s^*$ for constant charge boundary conditions and is zero for constant potential, and $(\Pi_{osm}^* - \Pi_{osm}^{*0})$ is $[\cosh(\psi^*) - 1]/\lambda^{*2}$ for the PB equation and is $\psi^{*2}/(2\lambda^{*2})$ in the DH approximation. $\xi_0(\eta)$ is defined by (Reiner, 1991):

$$\xi_0 = \cos^{-1}\left(\frac{d_1^*}{2\sqrt{(d_1^*)^2 - 3}}\right) + \cos^{-1}\left(\frac{\cosh[\eta - \cosh^{-1}(d_1^*/2)]}{\sqrt{(d_1^*)^2 - 3}}\right), \tag{22}$$

for the hexagonal subcell and is zero for an isolated pair of particles. N_c is the coordination number of the particle configuration, which is 1 for an isolated pair and 6 for the hexagonal cell. It is necessary to multiply the integrals in Eq. 21 by twice this factor since the integration limits are restricted in accordance with the symmetries of the two particle and lattice geometries.

The symmetric cell model may be treated similarly, but manipulations are simplified considerably by the fact that the potential ψ varies only in the radial direction r. If we scale r by the particle radius a, the outer boundary r_{max}^* of the cell may be fixed at:

$$r_{max}^* = r_v^* \equiv \frac{1}{\sqrt{\Phi}} = \frac{3^{1/4} d_1^*}{\sqrt{2\pi}}, \tag{23}$$

if it is desired that the cell's volume fraction agree with that of the hexagonal lattice, or at

$$r_{max}^* = r_d^* \equiv \frac{d_1^*}{2} = 3^{-1/4}\sqrt{\frac{\pi}{2\Phi}}, \tag{24}$$

for the "nearest neighbor" implementation of the model. Henceforth, these choices will be referred to as versions 1 and 2, respectively, of the cell model. The boundary condition on the potential at r_v^* or r_d^* is chosen as:

$$\frac{d\psi^*}{dr^*} = 0, \tag{25}$$

i.e., zero charge density, to mimic the symmetry conditions at the outer boundary of the full hexagonal cell.

In the DH limit (Eq. 5), it is possible to obtain an analytical expression for the interaction free energy of the cell model for both constant charge and constant potential boundary conditions. The solution to the scaled form of Eq. 5 subject to boundary condition (Eq. 25) is:

$$\psi^* = \lambda^* q_s^* \left[\frac{I_1(r_{max}^*/\lambda^*)K_0(r^*/\lambda^*) + K_1(r_{max}^*/\lambda^*)I_0(r^*/\lambda^*)}{I_1(r_{max}^*/\lambda^*)K_1(1/\lambda^*) - K_1(r_{max}^*/\lambda^*)I_1(1/\lambda^*)} \right] \tag{26}$$

for fixed surface charge density and

$$\psi^* = \psi_s^* \left[\frac{I_1(r_{max}^*/\lambda^*)K_0(r^*/\lambda^*) + K_1(r_{max}^*/\lambda^*)I_0(r^*/\lambda^*)}{I_1(r_{max}^*/\lambda^*)K_0(1/\lambda^*) + K_1(r_{max}^*/\lambda^*)I_0(1/\lambda^*)} \right] \tag{27}$$

for fixed surface potential. I_0 and I_1 are modified Bessel functions of the first kind, and K_0 and K_1 are modified Bessel functions of the second kind. It is possible, but extremely tedious, to evaluate Eq. 6 directly for these conditions. It is more convenient instead to utilize the special result that the free energy in the Debye-Hückel limit subject to linear boundary conditions may be reduced to surface integrals of the product of the charge density and potential (Reiner and Radke, 1990). For fixed charge conditions:

$$\Omega_e^{*\,cell} = \frac{1}{2}\int_S d\underline{r}^{s*} q_s^*(\underline{r}^{s*})\psi_s^*(\underline{r}^{s*}) = \pi q_s^* \psi_s^* = \pi\lambda^*(q_s^*)^2 \left[\frac{I_1(r_{max}^*/\lambda^*)K_0(1/\lambda^*) + K_1(r_{max}^*/\lambda^*)I_0(1/\lambda^*)}{I_1(r_{max}^*/\lambda^*)K_1(1/\lambda^*) - K_1(r_{max}^*/\lambda^*)I_1(1/\lambda^*)} \right], \tag{28}$$

while for fixed potential:

$$\Omega_e^{*\,cell} = \frac{-1}{2}\int_S d\underline{r}^{s*} q_s^*(\underline{r}^{s*})\psi_s^*(\underline{r}^{s*}) = -\pi q_s^* \psi_s^* = -\pi \frac{(\psi_s^*)^2}{\lambda^*} \left[\frac{I_1(r_{max}^*/\lambda^*)K_1(1/\lambda^*) - K_1(r_{max}^*/\lambda^*)I_1(1/\lambda^*)}{I_1(r_{max}^*/\lambda^*)K_0(1/\lambda^*) + K_1(r_{max}^*/\lambda^*)I_0(1/\lambda^*)} \right]. \tag{29}$$

To obtain the interaction free energy per particle $W_e^{*\,cell}$ for the cell model, it is necessary to subtract the free energy of an isolated particle, i.e., in the limit $r_{max}^* \to \infty$, from Eqs. 28 and 29:

$$W_e^{*\,cell}(r_{max}^*) \equiv \Omega_e^{*\,cell}(r_{max}^*) - \Omega_e^{*\,cell}(\infty) \tag{30}$$

These results become:

$$W_e^{*\,cell} = \frac{\pi(\lambda^* q_s^*)^2}{I_1(r_{max}^*/\lambda^*)K_1(1/\lambda^*) - K_1(r_{max}^*/\lambda^*)I_1(1/\lambda^*)} \times \left(\frac{K_1(r_{max}^*/\lambda^*)}{K_1(1/\lambda^*)}\right) \tag{31}$$

and

$$W_e^{*\,\mathrm{cell}} = \frac{\pi(\psi_s^*)^2}{I_1(r_{\max}^*/\lambda^*)K_0(1/\lambda^*)+K_1(r_{\max}^*/\lambda^*)I_0(1/\lambda^*)} \times \left(\frac{K_1(r_{\max}^*/\lambda^*)}{K_0(1/\lambda^*)}\right) \quad (32)$$

for the constant charge density and constant potential cases, respectively. While these analytical expressions are themselves useful, they are especially valuable for testing the correctness and accuracy of the approximate numerical techniques to be discussed below.

Although it is natural to employ cylindrical coordinates in expressing the free energy functional Ω_e for the symmetric cell model, it is particularly convenient to introduce a change of radial variables in numerical calculations. Asymptotically as $r^* \to \infty$, the potential ψ^* in the double layer surrounding an isolated cylinder obeys the Debye-Hückel scaling:

$$\psi^* \sim (r^*)^{-1/2}\exp(-r^*/\lambda^*) \quad (33)$$

while the contribution to the free energy from a differential shell dr^* at r^*:

$$d\Omega_e^* \sim -\pi dr^* r^* \left\{\left(\frac{d\psi^*}{dr^*}\right)^2 + \left(\frac{\psi^*}{\lambda^*}\right)^2\right\} = -2\pi dr^* \exp(-2r^*/\lambda^*) \times \left\{(\lambda^*)^{-2} + \frac{1}{2}(\lambda^* r^*)^{-1} + \frac{1}{8}(r^*)^{-2}\right\}. \quad (34)$$

decays exponentially with r^*. Since it is computationally inefficient (at small volume fractions) to represent the potential uniformly over a region of which only a minute portion dominates the free energy, we choose a new independent variable:

$$\zeta \equiv 1 - \exp((1-r^*)/\lambda^*) \quad (35)$$

which maps the particle surface at $r^* = 1$ into $\zeta = 0$ and $r^* = \infty$ into $\zeta = 1$. The free energy functional may be expressed in terms of this coordinate as:

$$\Omega_e^{*\,\mathrm{cell}} = 2\pi\left\{\omega_s^* - \int_0^{\zeta_{\max}} d\zeta(1-\lambda^*\ln(1-\zeta)) \times \left[\frac{(1-\zeta)}{2\lambda^*}\left(\frac{d\psi^*}{d\zeta}\right)^2 + \frac{\lambda^*}{(1-\zeta)}(\Pi_{\mathrm{osm}}^* - \Pi_{\mathrm{osm}}^{*0})\right]\right\}, \quad (36)$$

where $\zeta_{\max}$ is defined in terms of $r_{\max}^*$ by the transformation (Eq. 35). This change of variables is advantageous for numerical work because regions of equal size in ζ contribute approximately equally to the free energy.

Previous studies of electrostatic interactions between systems of cylindrical particles have been restricted for the most part to either the pair or cell approximations. Dube (1943) calculated two-particle energies for constant surface charge conditions via a linear superposition approach. Sparnaay (1959) applied Derjaguin's (1934, 1939) lubrication technique and Levine's (1934, 1939b) multipole expansion to obtain approximate pair potentials for cylinders at constant surface potential in the DH theory. Lifson and Katchalsky (1954) utilized a charging process to derive the free energy of the cell model from the exact solution to the nonlinear PBE in cylindrical coordinates obtained by Fuoss et al. (1951) and Alfrey et al. (1951) for constant charge conditions. These results were limited to the case of no added electrolyte. Alexandrowicz (1962), Alexandrowicz and Katchalsky (1963), and Einevoll and Hemmer (1988) have used perturbative techniques to extend the calculations of Fuoss et al. and Alfrey et al. to include small amounts of added salt. These studies proceeded only to the calculation of the excess osmotic pressure at the cell boundary, which is equal to the external force necessary to stabilize the cell. Parsegian (1964) utilized Lifson and Katchalsky's expressions for W_e to construct a theory of the formation of hexagonal liquid crystal phases. Elliott (1968) followed Parsegian's approach and applied Derjaguin's method to the nonlinear PBE as well, to attempt to explain the crystallization of TMV. Brenner and McQuarrie (1973b, c) used the multipole expansion method to obtain the free energy of interaction in the DH approximation between pairs of cylinders bearing amphoteric surface groups.

Only in the last decade has the hexagonal model been investigated. Millman and Nickel (1980) and Millman et al. (1984) introduced the model and expanded the electrostatic potential in Eq. 4 around a central particle as a series of radially-dependent functions multiplied by harmonics satisfying the twelvefold symmetry condition of the hexagonal cell. They then solved the resulting system of equations subject to conditions of constant charge density at the particle surface and symmetry of the potential at the outer boundary of the cell. In their work, configurational free energies were not calculated directly, nor was any attempt made to compare sums of pair potentials or the interaction energy from the symmetric cell model to the exact results. More recently, Guldbrand et al. (1986) performed Monte Carlo simulations for a model of finite-sized ions surrounding a cylinder at fixed surface charge in a hexagonal cell and compared the ionic distribution functions and osmotic pressure at the outer boundary obtained from their computations to the predictions of the PB equation for the radially-symmetric model. These calculations complement the extensive Monte Carlo data available in the literature (Le Bret and Zimm, 1984; Mills et al., 1985; Vlachy and Haymet, 1986) for finite-sized ionic models in cylindrical geometry.

Variational/Finite Element Solution

Although the calculus of variations is a convenient route to the derivation of the configurational free energy functional from models for the ionic distribution functions, its power becomes most apparent when the method is coupled with a numerical procedure for approximating the potential over the region of interest. If a trial function containing a finite number p of variable parameters $\{\alpha_j; j = 1, \ldots, p\}$ is chosen, the discrete analogues of the Euler-Lagrange equations:

$$\frac{\partial \Omega_e^*}{\partial \alpha_j} = 0; j = 1, \ldots, p \quad (37)$$

establish a clear criterion for the optimal values of those constants. More importantly, if the difference between the exact potential and the approximation is small, then the variational principle for Ω_e^* guarantees that an error proportional to a constant ϑ in the potential will appear only to order ϑ^2 in the

free energy (Reiner, 1991). This property makes the variational approach a particularly attractive means for obtaining approximate values of configurational free energies in numerical calculations.

The approximation technique chosen in this study is the finite element method. The trial potential is chosen as a linear combination of variable parameters multiplied by simple, spatially localized basis functions:

$$\psi^*(\underline{r}^*) = \sum_{j=1}^{p} \alpha_j \phi_j(\underline{r}^*). \tag{38}$$

In the cylindrical and bipolar coordinate calculations, the bases ϕ_j were chosen as linear (in ζ) and bilinear (in ξ and η) functions, respectively (Strang and Fix, 1973; Mori, 1986). Solutions were converged using Newton's method. Matrix inversion for the two-dimensional (bipolar) computations was performed using a conjugate gradient method (Wolfe, 1978; Bertsekas, 1982; Press et al., 1986).

Numerical evaluation of W_e^* for the cell, hexagonal, and pair calculations requires that a procedure analogous to the transformation from Eqs. 28 and 29 to Eqs. 31 and 32 be followed. First, functionals for Ω_e^* (Eq. 21 or 36) at the values of Φ (or d_1^* or ζ_{max}), λ^*, and q_s^* or ψ_s^* of interest must be extremized with respect to the parameters $\underset{\sim}{\alpha}$; then, the interaction free energy may be obtained by subtracting the corresponding value of Ω_e^* in the limit of large interparticle separations. Additionally, for the calculation of the free energy per particle in the pair approximation, it is necessary to perform the summation over shells of neighbors in Eq. 11. All of the results to be presented here are based on the restriction of this sum to the 11 shells shown in Table 1. That number was sufficient to secure convergence of the free energy per particle except for calculations at large Debye lengths; the failure of the sum to converge under those conditions will be examined in more detail in the results section where those computations are discussed.

For the cell model calculations, the region from $\zeta = 0$ to ζ_{max} was subdivided uniformly into 2,500 elements, so that the potential was represented by a basis consisting of 2,501 parameters. Reference values of Ω_e^* were obtained by extremizing Eq. 36 with ζ_{max} set equal to one minus a small constant. For computations performed in the Debye-Hückel limit, the resulting values of W_e^* were compared to the exact solutions in Eqs. 31 and 32; all free energies agreed to at least six significant digits.

In the calculations done for pair and hexagonal geometries, a division of the (ξ, η) region into 2,500 elements was also selected. Initially, a choice of a 50 by 50 grid was made. However, we realized that a useful property of the variational principle for the free energy is that Ω_e^* may be optimized not only with respect to the coefficients in the expansion (Eq. 38), but also with respect to the distribution of elements. Thus, for each set of parameters studied, the maximum value of Ω_e^* was chosen from results for 10 by 250, 25 by 100, 50 by 50, 100 by 25, and 250 by 10 grids. In practice, such an extensive set of computations was not necessary; since the best choice of grids varies uniformly as individual physical values are changed, only one or two calculations were required for each set of parameters. It also proved convenient to choose a slightly nonuniform distribution of elements to improve the accuracy of the approximated potential near the particle surface and to eliminate the Debye length dependence of the optimal selection of grids. Details are available elsewhere (Reiner, 1991).

We believe that the primary limit to the precision of our calculations is the subtraction of the free energy of an isolated particle from Ω_e^* discussed above. On the scales displayed in the figures below, the hexagonal values for W_e^* are correct to within the maximum of absolute or relative errors of approximately 2×10^{-5} under most conditions, while the maximum error in the sum of pair potentials is about an order of magnitude greater. These deviations are a factor of 10 larger at $\lambda^* = 0.1$ and the same factor smaller at $\lambda^* = 10$, and are nearly independent of surface charge density and potential in the regime examined here. For ψ_s^* near 10, however, compaction of the double layer near the particle surface has the same effect on precision as reduction of the Debye length, and approximately another significant digit is lost.

Several techniques to maximize the robustness and efficiency of our code were employed. In studies of series of parameter values, up to five previous converged solutions were used to construct an initial guess for each calculation. Armijo's rule (Bertsekas, 1982) was used to stabilize Newton's method for the most strongly nonlinear cases when no such estimate was available. Details of implementation and convergence properties are presented in the thesis of Reiner (1991).

Results

To test comprehensively the accuracy of the pair and cell approximations, it is necessary to vary independently each of the physical parameters that characterize our model for electrostatic interactions. There are three such parameters for this system: the volume (or area) fraction Φ, the ratio of the Debye length to the particle radius λ^*, and the scaled surface charge density q_s^* or surface potential ψ_s^*. In this section, we vary each of these dimensionless quantities individually and examine their effect on the validity of the approximate methods.

As may be observed from Eqs. 28 to 32, electrostatic free energies are proportional to the square of q_s^* or ψ_s^* in the Debye-Hückel limit. Accordingly, all values of W_e^* for fixed surface charge density and potential are rescaled with $(q_s^*)^2$ or $(\psi_s^*)^2$, respectively. Further, in the constant charge case the interaction energy (Eq. 31) scales as $(\lambda^*)^2$ in the limit of large Debye lengths, while for constant potential, Eq. 32 behaves as $1/\log(\lambda^*)$. It was, therefore, found convenient to divide all fixed charge results by $(\lambda^*)^2$; no Debye length-dependent rescaling was chosen for fixed surface potentials.

Variations of volume fraction

In the first set of calculations, we investigate the scaled interaction free energy W_e^* as the particle volume fraction is varied from 0 to 0.8717 (96% of the closest packing value 0.9069). λ^* is set equal to one for this portion of the study, since it is in this regime that the interplay of double-layer overlap and particle geometry is most interesting. At smaller Debye lengths, the individual double layers are of minimal extent and particle interactions are extremely localized, while at larger λ^*, interactions become so long-ranged that a pair, potential-based description of the system is not meaningful; this issue will be examined further when variations of the Debye

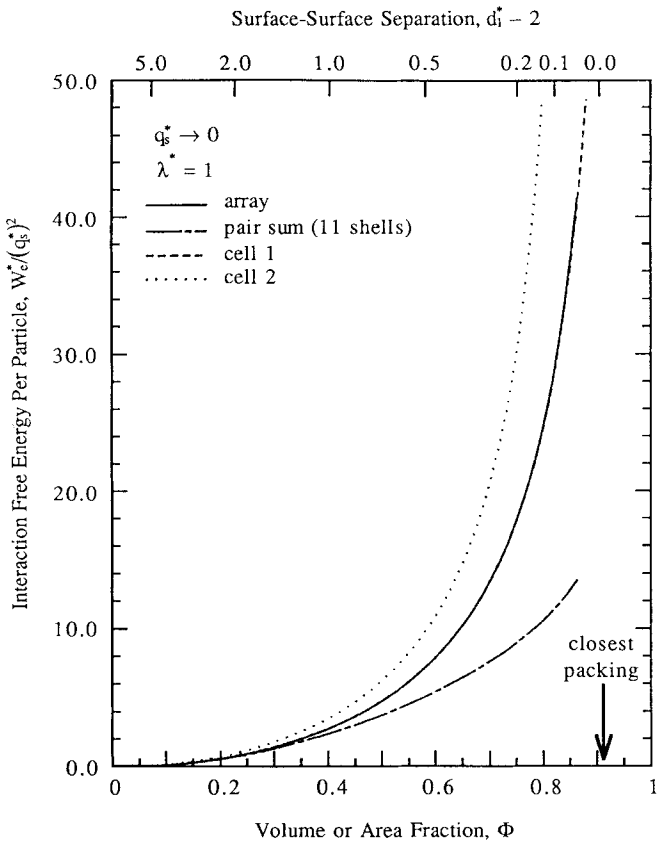

Figure 4. Dimensionless free energy per particle, $W_e^*/(q_s^*)^2$, vs. volume (or area) fraction, Φ, and surface-surface separation, $d_j^* - 2$, for constant surface charge conditions in the Debye-Hückel limit $q_s^* \to 0$.

The Debye length λ is equal to the particle radius a in Figures 4-8.

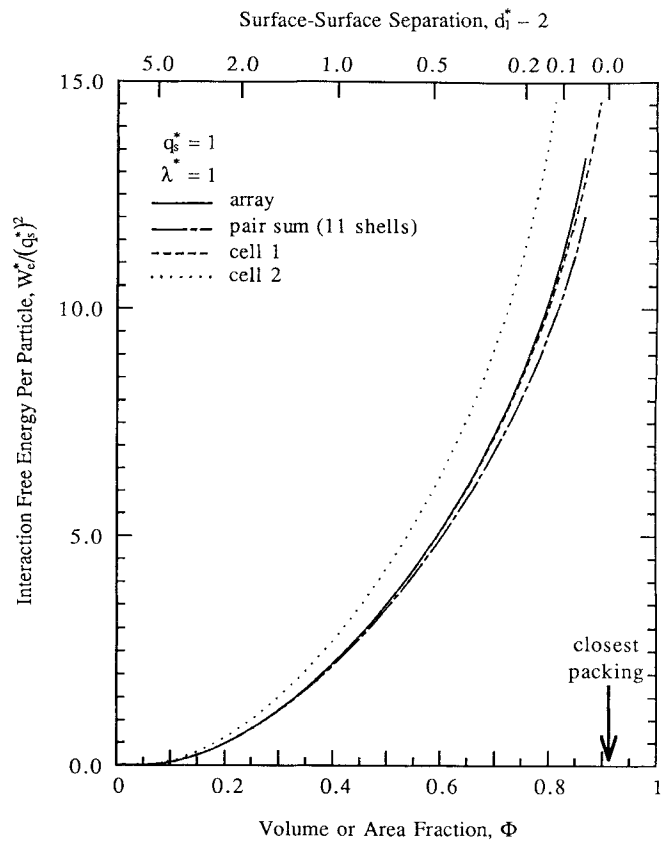

Figure 5. Dimensionless free energy per particle, $W_e^*/(q_s^*)^2$, vs. volume (or area) fraction, Φ, and surface-surface separation, $d_j^* - 2$, for an intermediate fixed surface charge density, $q_s^* = 1$.

length are discussed. We consider three cases each of fixed surface charge density and potential: (1) the DH limit of q_s^* or $\psi_s^* \to 0$; (2) intermediate charge density q_s^* or potential $\psi_s^* = 1$, where some nonlinear effects are expected to appear; and (3) large q_s^* or $\psi_s^* = 10$, where the potential within one Debye length of the particle surface is expected to decay much faster than in the DH limit. Qualitatively, all of the approximations should be accurate at small volume fractions, where double-layer overlap and detailed aspects of particle geometry are unimportant. The predictions of the pair and first cell models should worsen as closest packing is approached, whereas the second cell model should become more accurate.

Figure 4 displays results for the free energy per particle at constant charge density in the Debye-Hückel limit as a function of Φ for the hexagonal lattice and the three approximate models. At 25% of closest packing ($\Phi = 0.2267$), the sum of pair potentials underestimates the true free energy by less than 4%, but worsens steadily as the volume fraction increases, erring by nearly 18% at 50% and by more than 40% at 75% of maximum packing. Remarkably more faithful predictions are made by the first cell model, which errs by less than 1% for all volume fractions considered here and by less than 0.1% for volume fractions less than 75% of closest packing. The second implementation is qualitatively, but not quantitatively correct, throughout.

Quite different behavior appears in Figure 5 for $q_s^* = 1$. The pair approximation underestimates the hexagonal free energy by only 1.0%, 2.4%, and 4.7% at 25%, 50%, and 75% of closest packing, and by less than 10% even at 96% of closest packing. The first cell model is again extremely accurate for all conditions, underestimating the correct value of the free energy by less than 0.5% for all volume fractions below 75% of closest packing, and erring by less than 4% at the maximum particle density considered here; the second cell model is again in only qualitative agreement. It is noteworthy in comparing Figures 4 and 5 that the nonlinearity of the PB equation for this charge density reduces the magnitude of particle interactions by a factor of nearly two at 75% and by four at 96% of maximum packing.

At a dimensionless charge density of 10 in Figure 6, it now appears that the pair approximation is invalid for all but the smallest volume fractions; by 25% of closest packing it is already in error by more than 20%. Particularly interesting, however, is the observation that it now *overestimates* the free energy per particle. The sum of pair potentials steadily worsens up to $\Phi \cong 0.75$, where it begins to improve slightly as the divergence of the interaction between nearly touching particle surfaces dominates the electrostatic free energy. The first version of the cell model remains quite accurate, underestimating the free energy by less than 1% below 50% of closest packing, and by only 9% at the largest particle concentrations considered here. The magnitude of nonlinear effects for this surface charge density may be judged from the fact that the lattice

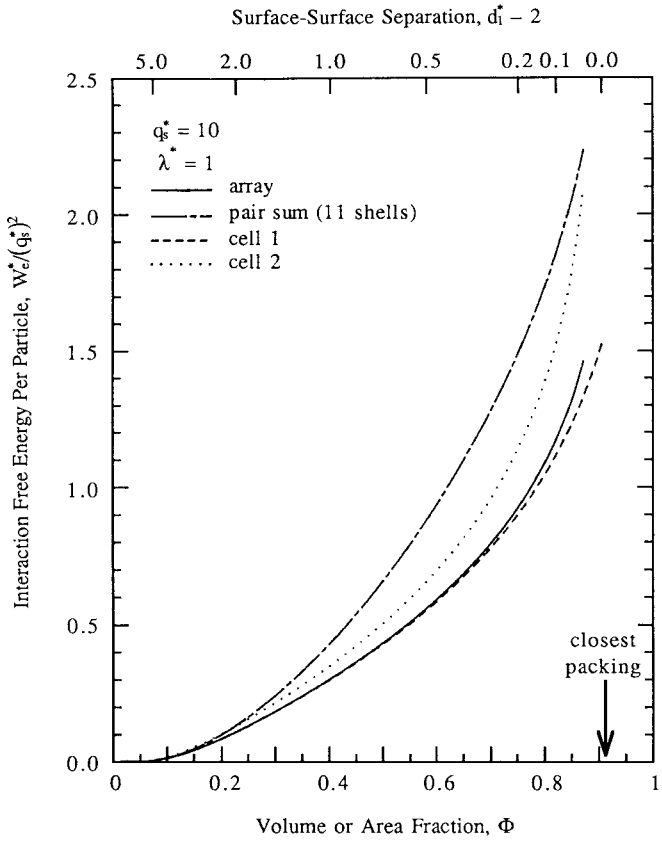

Figure 6. Dimensionless free energy per particle, $W_e^*/(q_s^*)^2$, vs. volume (or area) fraction, Φ, and surface-surface separation, $d_1^* - 2$, for a large fixed surface charge density, $q_s^* = 10$.

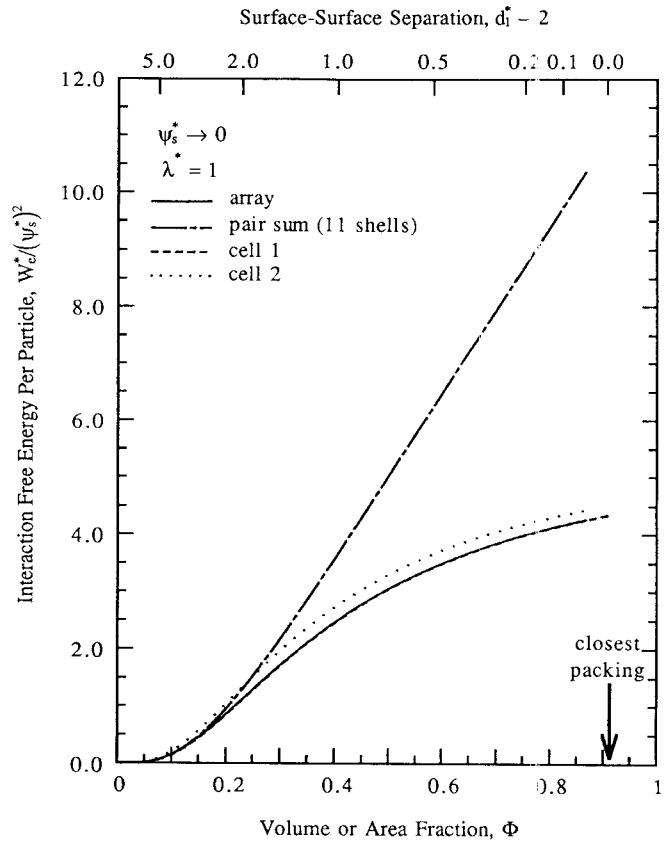

Figure 7. Dimensionless free energy per particle, $W_e^*/(\psi_s^*)^2$, vs. volume (or area) fraction, Φ, and surface-surface separation, $d_1^* - 2$, for constant surface potential in the Debye-Hückel limit $\psi_s^* \to 0$.

and cell interactions are reduced by a factor of nearly 30 from their Debye-Hückel values at $\Phi = 0.8717$ and by approximately 4 at large interparticle separations. We remind the reader that the interaction free energies are nevertheless monotonically increasing functions of q_s^*, since W_e^* is proportional to the square of the surface charge density in the DH limit.

The qualitative behavior of the results shown in Figures 4–6 as particle concentrations are increased is much the same as anticipated: the sum of pair potentials approximates the electrostatic free energy of the hexagonal lattice well at small volume fractions, but worsens steadily as the particle concentration is increased and the overlap of multiple double layers becomes important. The superb accuracy of the first version of the cell model is, perhaps, not so easily foreseen, but implies that the details of configurational geometry are not important except at very small separations. However, the trend to increased and then decreased accuracy of the pair approximation as the surface charge is raised was entirely unexpected and will be examined more closely in the last section of results, where q_s^* is varied at constant Φ and λ^*.

The opposing pole of surface conditions is that of constant potential, for which results as the volume fraction is varied are shown in Figures 7 and 8. Interaction free energies for $\psi_s^* = 1$ are not presented here since they are nearly identical to those for $\psi_s^* \to 0$ in Figure 7, differing by a maximum of 3% at conditions approaching closest packing. This similarity confirms that the DH approximation is quite accurate at even moderate surface potentials.

The pair approximation for low and intermediate surface potentials is useful only for volume fractions less than 25% of closest packing, by which point the pair sum overestimates W_e^* by 15%. As in the constant charge cases examined earlier, this approximation becomes substantially worse as the particles are brought together, erring by approximately 50% and 100% at 50% and 75% of closest packing. In contrast to the fixed q_s^* calculations, in which the interaction free energy diverges as charged surfaces approach each other, W_e^* here approaches a constant limiting value at contact when ψ_s^* is held constant and the charge density on two nearly touching surfaces falls to zero. The pair results are nearly linear for $\Phi > 0.2$ and overestimate the free energy per particle by 150% in the close-packed limit. The hexagonal and cell results approach their asymptotic values with much smaller slopes; indeed, the predictions of the first cell model are essentially indistinguishable from those of the hexagonal lattice, underestimating interactions by less than 0.1% even at contact. The second cell model performs better here than for the constant charge cases since the electrostatic free energy remains almost constant for large particle densities, but never challenges the accuracy of the first implementation.

For the large surface potential case $\psi_s^* = 10$ presented in Figure 8, the double layer is concentrated very near the particles' surfaces, causing the contact values of W_e^* to be ap-

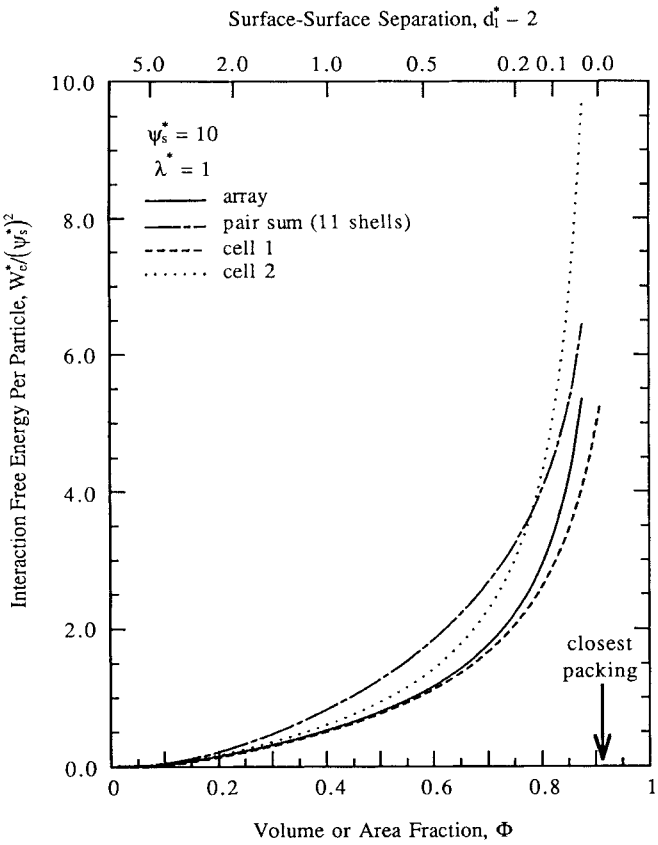

Figure 8. Dimensionless free energy per particle, $W_e^*/(\psi_s^*)^2$, vs. volume (or area) fraction, Φ, and surface-surface separation, $d_1^* - 2$, for a large fixed surface potential, $\psi_s^* = 10$.

proached much more slowly as Φ is increased, and leading to very interesting behavior. The pair approximation actually improves at high concentrations. Since interactions between nearly touching particles dominate the free energy, double-layer overlap becomes a secondary consideration under these conditions. Quantitatively this trend is clear: the pair sum errs by 45% at 25% of closest packing, by 58% at 50%, by 53% at 75%, and by 20% at 96%. The cell model works well up to fairly high particle densities, underestimating the array free energy by 5% at 75% of closest packing. At $\Phi = 0.8717$, however, this approximation is actually worse than the pair sum, underestimating W_e^* by nearly 25%. The second cell model displays the qualitative features of the exact solution but never improves quantitatively, erring by nearly 100% as closest packing is approached. It does, however, provide an upper bound to the correct free energy of interaction.

Interpretation of the results in Figures 7 and 8 is reasonably straightforward. At small and moderate values of ψ_s^*, the electrostatic potential decays uniformly as one moves away from particle surfaces. Thus, interactions vary smoothly with particle separations and the first cell model approximates the free energy of the hexagonal array well, since geometric details of particle configurations are effectively washed out. At large surface potentials, the double layer is compacted near each particle. Thus, at small concentrations, $W_e^*/(\psi_s^*)^2$ is much smaller than for small ψ_s^*, since potentials far away from particle surfaces are a much smaller fraction of the surface potential. At large Φ, however, regions of the double layer at high potential interact, and the exponential contribution (Eq. 7) to the osmotic pressure dominates, leading to stronger repulsion than in the low potential limit. The pair sum consistently overestimates free energies for fixed potential cases, since multiparticle interactions have the effect of lowering the surface charge to maintain constant ψ_s^*. These interactions become less important as the particle density is increased, leading to improvement of the pair approximation. In contrast, the first cell model underestimates the free energy of the hexagonal cell at large potentials because it does not reproduce the strong repulsion between charged surfaces near contact, while the second version of the model overpredicts W_e^* since it effectively assumes that all neighboring particle surfaces are located at the distance of closest approach; geometric details do become important at large potentials.

Variations of Debye length

The second physical parameter examined in our study is the Debye length λ^*. Variations of this parameter are of interest for two reasons: first, because its value may be altered under experimental conditions through the addition of electrolyte to the solvent in which the particles are suspended; and second, because changes in the Debye length are distinct from the purely geometrical effects caused by changing particle concentrations. Qualitatively, we expect results similar to those for variations of volume fraction: both the pair and cell models should be quite accurate when λ^* is much smaller than typical interparticle distances. At larger values of the dimensionless Debye length, the pair approximation should become poor, since the double layer surrounding each particle overlaps with those of particles far away from it. Under these circumstances, it is not useful to consider interactions between pairs of particles, since the electrostatic free energy of a suspension becomes an inherently many-body quantity. For such conditions it seems reasonable to predict that only the cell models would provide useful approximations to the exact value of W_e^*.

We chose to vary λ^* from 0.1 to 10.0 for the same values of q_s^* and ψ_s^* considered in the study of concentration effects discussed above. Moreover, we fixed Φ at 50% of closest packing ($d_1^* = 2\sqrt{2}$) to eliminate effects due purely to the closeness of particle surfaces, while maintaining the density of particles large enough to observe electrolyte and surface charge- or potential-dependent phenomena for the ranges of λ^* considered here. We found, however, that conditions of $\psi_s^* = 10$ and $\lambda^* < 0.25$ so localized the double layer near the particle surface that it became extremely difficult to obtain accurate numerical values of W_e^*, particularly for the pair calculations. Accordingly, we do not present results for $\psi_s^* = 10$ here. As discussed earlier in this section, it is convenient to divide the free energy for constant charge calculations by $(\lambda^*)^2$.

Results for the Debye-Hückel limit $q_s^* \to 0$ are displayed in Figure 9. In the limit of large λ^*, the hexagonal and cell free energies increase proportionally to $(\lambda^*)^2$, as expected from Eq. 31. The pair results increase more slowly because the effects of double-layer overlap are smaller for an isolated pair of particles; the surface potential of each rises significantly over only a small region as another particle is brought close to it. As expected, the pair sum is poor for $\lambda^* > 1$, where it underestimates W_e^* by more than 15%. At $\lambda^* = 10$, this error has

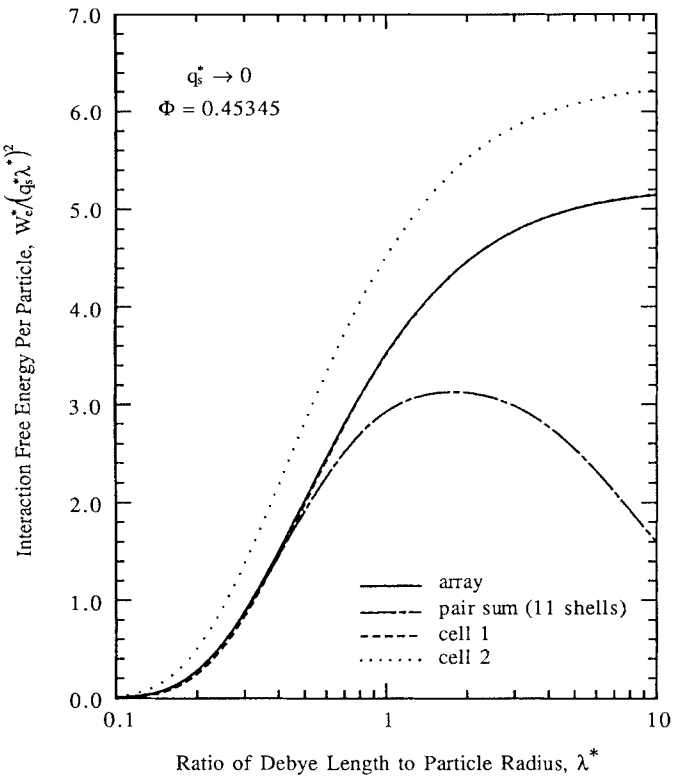

Figure 9. Dimensionless free energy per particle, $W_e^*/(q_s^*\lambda^*)^2$, vs. ratio of Debye length to particle radius, λ^*, for constant surface charge conditions in the Debye-Hückel limit $q_s^* \to 0$.

The volume fraction is equal to half its closest packed value in Figures 9-12.

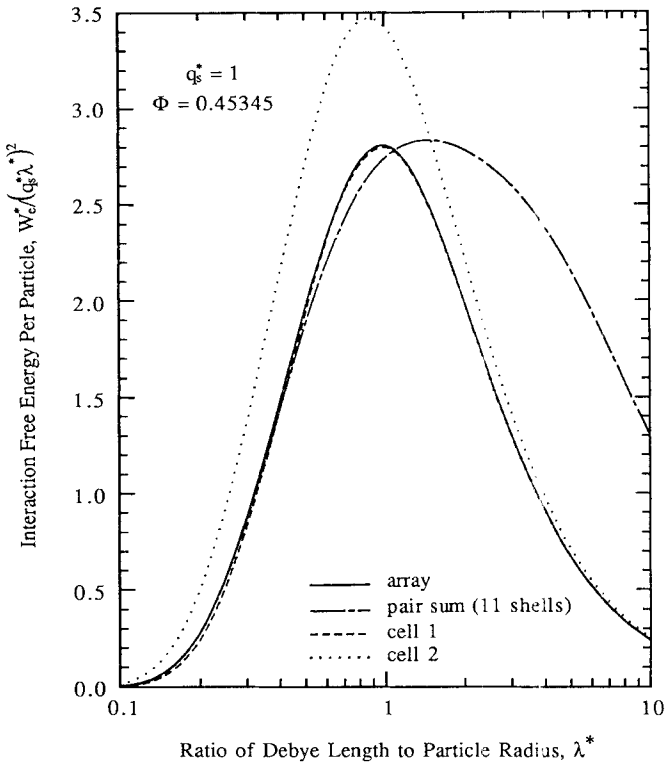

Figure 10. Dimensionless free energy per particle, $W_e^*/(q_s^*\lambda^*)^2$, vs. ratio of Debye length to particle radius, λ^*, for an intermediate fixed surface charge density, $q_s^* = 1$.

increased to nearly 70%. The accuracy of this approximation improves steadily as the Debye length is decreased, erring by less than 1% for $\lambda^* < 0.25$. The first cell model is excellent for $\lambda^* > 1$, underestimating the exact free energy per particle at that Debye length by 0.3% and improving to greater than five digits of accuracy by $\lambda^* = 10$. Curiously, where the pair approximation fares well, the cell model does quite poorly: although difficult to discern in the figure, for λ^* less than 0.2 it is too low by more than 13% and is incorrect by more than 40% at $\lambda^* = 0.1$. Our initial explanation for these results was to ascribe them to the subtraction of the free energy of the hexagonal lattice at infinite dilution. However, the difference between that value of $\Omega_e^*(\infty)$ and the exact value for an isolated cylinder was only 3% of W_e^* for the array at $\lambda^* = 0.1$ and less than 0.03% at $\lambda^* = 0.2$. Thus, this discrepancy could not have resulted from computational inaccuracy. We believe that the correct explanation of this phenomenon may be derived from the observation that at very small Debye lengths the electrostatic potential varies strongly with distance from the particle surface. Consequently, it is critical to reproduce the positions of the surfaces of nearest neighbors to obtain an accurate value of the configurational free energy. Since the overlapping of multiple double layers is minimal and neighbors beyond the first shell contribute little to the sum of pair potentials, the pair approximation is quite good. The cell model, however, does not represent details of configurational geometry, and hence, does poorly. The second cell model remains qualitatively correct for these conditions, but consistently overestimates the free energy.

At a dimensionless surface charge density of 1, represented in Figure 10, much the same qualitative behavior as in Figure 9 holds for $\lambda^* < 1$, since the corresponding surface potentials are small for short Debye lengths and the DH approximation is valid. At larger λ^*, the nonlinearity of the Poisson-Boltzmann equation causes the surface potential to grow more slowly than linearly as q_s^* is increased, so that W_e^* also grows at a slower than quadratic rate. This saturation of ψ_s^* also implies that the approach of additional particles to the vicinity of an isolated pair produces less repulsion than between individual pairs. Thus, the pair free energy begins to overestimate W_e^* for $\lambda^* > 1$, instead of underestimating it by neglecting the increase in surface potential due to multiple double layer overlap. The balance of these two effects causes the pair approximation to improve slightly as λ^* rises from 0.5 to 1.0, and then to worsen drastically as it is increased further. By $\lambda^* = 10$, the pair sum is too large by more than 450%, although it retains better than 10% accuracy for dimensionless Debye lengths less than 0.25. The first cell model is good to within 0.4% at $\lambda^* = 1$ and 0.05% at $\lambda^* = 10$. The second implementation of the model overestimates W_e^* everywhere, but becomes more accurate as the Debye length increases since ψ varies more slowly with distance. At $\lambda^* = 10$, it is in error by less than 5%.

At $q_s^* = 10$, shown in Figure 11, the pair sum is larger than the exact value of W_e^* for all $\lambda^* > 0.25$; it is of better than 1% accuracy for all smaller Debye lengths. It is too large by more than 10% by $\lambda^* = 0.5$, nearly 50% by $\lambda^* = 1$, and almost 7 times greater than the correct value at $\lambda^* = 10$. The first cell

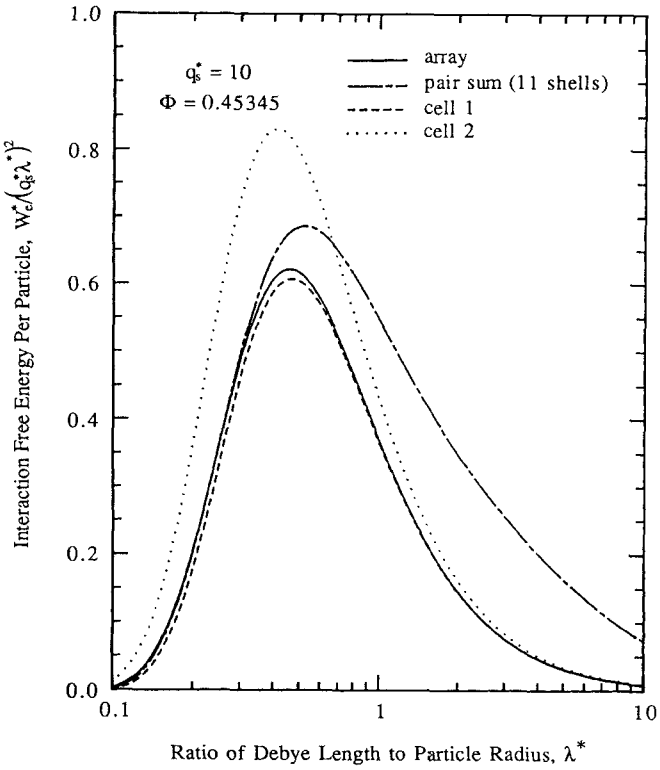

Figure 11. Dimensionless free energy per particle, $W_e^*/(q_s^*\lambda^*)^2$, vs. ratio of Debye length to particle radius, λ^*, for a large fixed surface charge density, $q_s^* = 10$.

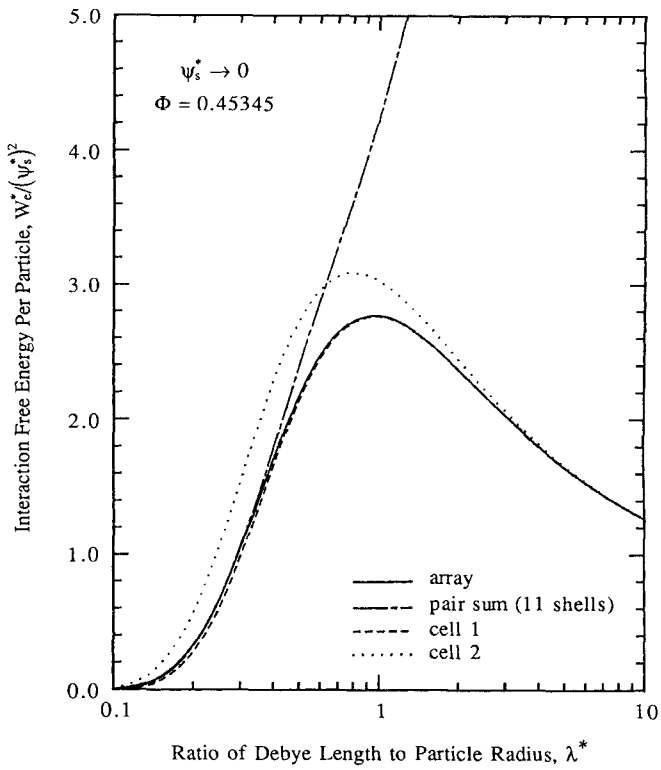

Figure 12. Dimensionless free energy per particle, $W_e^*/(\psi_s^*)^2$, versus ratio of Debye length to particle radius, λ^*, for constant surface potential in the Debye-Hückel limit $\psi_s^* \to 0$.

model free energy is still too small by nearly 45% at $\lambda^* = 0.1$, but recovers its accuracy much more slowly than at lower surface charges since ψ varies more strongly with distance. Only by $\lambda^* = 1$ does it agree with the exact array results to better than 1%. The second cell model also improves steadily as the Debye length increases, but still overestimates W_e^* by 5% at $\lambda^* = 10$.

The results for the constant potential conditions $\psi_s^* \to 0$ and $\psi_s^* = 1$ are, again, very similar, differing by only a few percent even at $\lambda^* = 0.1$. Accordingly, we choose to display only the free energies for the low potential limit in Figure 12. The qualitative characteristics of the agreement between the approximate models and the exact solution are much the same as for the constant charge cases discussed above: the sum of pair potentials is accurate to better than 1% for $\lambda^* < 0.25$, but worsens drastically as the Debye length is increased, overestimating W_e^* by more than 10% at $\lambda^* = 0.5$ and by over 50% at 1.0. Indeed, the interaction free energy for the array and the cell models approaches zero as $1/\log(\lambda^*)$ in the limit of large Debye lengths, while the pair sum diverges! This behavior derives from the long-ranged character of the potential in this limit: particles many radii apart still repel one another strongly. In fact, the eleventh shell of neighbors contributes over 3% of the sum to that point. The array and cell values for W_e^* remain finite for λ^* large, because the presence of surfaces at fixed ψ_s^* surrounding a central particle causes its surface charge density to decrease as the extent of the double layer increases. Although more distant shells of neighbors also contribute significantly to the pair sum at constant q_s^*, the enormous disparity between the pair and array free energies is not observed in our fixed charge density calculations, since the strength of repulsion between two or more double layers increases with q_s^* as the surface potential rises proportionally. In contrast, in the fixed potential case, the approach of additional particles to the vicinity of an isolated pair has a diminished effect on their surface charge. Since the pair approximation does not correct for this reduction, it diverges wildly.

The first cell model agrees with the array free energy to within 10% by $\lambda^* = 0.25$, to nearly 1% and 0.1% at $\lambda^* = 0.5$ and 1.0, and to six significant digits at a dimensionless Debye length of 10. As λ^* is lowered, the cell model worsens steadily for the same reason as in the constant charge cases in Figures 9–11; at $\lambda^* = 0.1$ it is too low by more than 40%. The second version of the cell model's prediction exceeds the correct W_e^* by 150% at these conditions, but improves substantially as the Debye length grows, remaining too large by 9% at $\lambda^* = 1.0$ and by only 0.25% at $\lambda^* = 10$. This improvement results from the very slow variation with separation distance of the free energy of the array and the cell models, as in Figure 7. The electrostatic potential ψ is so long-ranged for large Debye lengths that it matters little whether the outer boundary of the cell is located at $r_{max}^* \approx 1.485$ or 1.414. We were rather startled by the appearance of a maximum in W_e^*, even though it might have been anticipated from the asymptotic behavior of the cell model noted previously. We will return to this topic in the discussion section.

Variations of surface charge density and potential

The third set of parameters for which we performed cal-

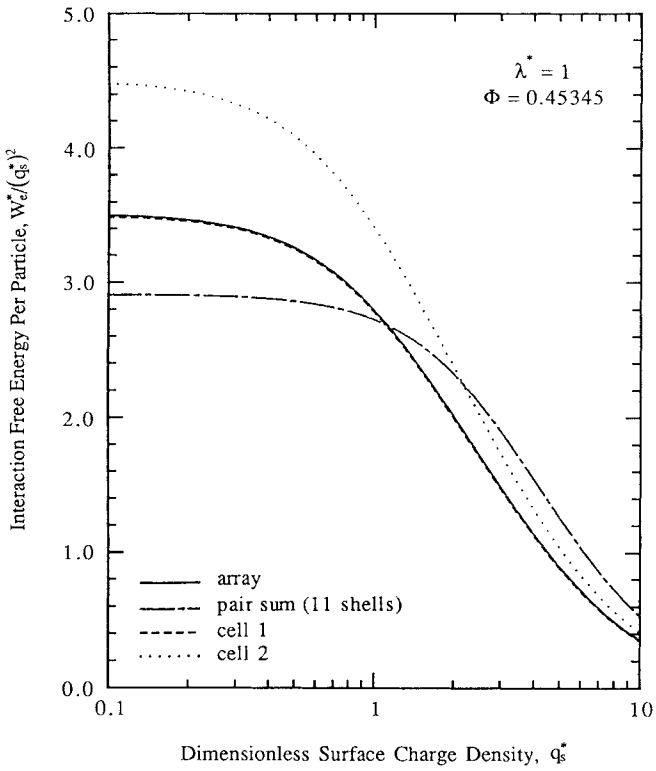

Figure 13. Dimensionless free energy per particle, $W_e^*/(q_s^*)^2$, vs. dimensionless surface charge density, q_s^*, for fixed charge conditions at $\lambda^* = 1$ and a volume fraction, Φ, equal to half its closest packed limit.

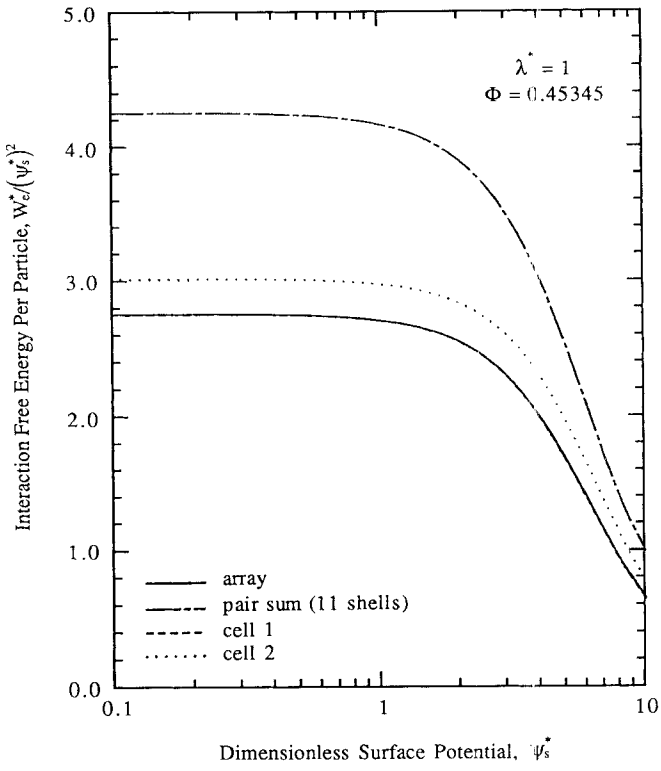

Figure 14. Dimensionless free energy per particle, $W_e^*/(\psi_s^*)^2$, vs. dimensionless surface potential, ψ_s^*, for fixed potential conditions at $\lambda^* = 1$ and a volume fraction, Φ, equal to half its closest packed limit.

culations is the surface charge density q_s^* and potential ψ_s^*. We chose to vary each of these over the interval 0.1 to 10.0, fixing the volume fraction at 0.4534 as for our Debye length studies and holding λ^* constant at 1.0 as for the variations of volume fraction. We were particularly interested in obtaining a better understanding of the complex relation between surface conditions and the accuracy of the pair approximation reflected in Figures 4-6 and 7-8.

Figure 13 shows the values of W_e^* [divided by $(q_s^*)^2$] for fixed surface charge density. At small values of q_s^*, each free energy smoothly approaches Debye-Hückel scaling, while for $q_s^* > 1$, each grows nearly linearly. The transition of the pair approximation from overprediction of W_e^* at low charges to agreement for q_s^* near 1 and thence to underestimation is more apparent here than in Figures 4-6. At a dimensionless charge density of 0.1, the sum over pairs is too low by 17%. By $q_s^* = 1$, it is only 2.4% smaller than the exact value. Thereafter, it begins to exceed the free energy of the array, erring by 48% at $q_s^* = 10$. Cell model one follows W_e^* of the hexagonal configuration closely and is off by less than 1% for all charge densities. The second cell model improves slightly as q_s^* is raised, predicting interactions too large by 28%, 22%, and 18% at $q_s^* = 0.1$, 1.0, and 10, respectively. At large charge densities, the surface potential has saturated, and the approach of the outer boundary of the cell toward the particle surface has a slightly reduced effect on the free energy of the double layer.

The sum of pair interactions consistently exceeds the free energy of the array for the fixed surface potential variations shown in Figure 14. At all values of ψ_s^* considered in these calculations, it is too large by 50 to 55%. As in the constant q_s^* computations, the first cell approximation remains valid everywhere and is correct to within 1% up to dimensionless potentials of 5. Its predictions worsen slightly thereafter, erring by about 2% at $\psi_s^* = 10$. At such large surface potentials, the electrostatic potential within the double layer still varies strongly half a Debye length away from the particle surface, causing details of configurational geometry to have some influence on the free energy. All values of W_e^* for $\psi_s^* < 1$ scale essentially as the Debye-Hückel limit $(\psi_s^*)^2$, while they grow at a rate between linear and quadratic for large surface potentials.

It is somewhat challenging to interpret the pair results shown in Figure 13. At low charge densities, the pair approach fails to reproduce the rise in surface potentials caused by interaction of multiple double layers, thereby underestimating W_e^*. As q_s^* is increased, the nonlinearity of the hyperbolic sine in Eq. 13 begins to dominate the decay of the potential near the particle surface, and growth of ψ_s^* is thereby limited. By $q_s^* = 10$, therefore, particles are effectively interacting at constant surface *potential*. Since the pair approximation overestimates potentials within the double layer for such conditions, its predictions for the interaction free energy are consequently too large. The agreement between the sum of pair interactions and the results for the hexagonal array displayed in Figure 5 is thus a fortuitous consequence of the balance between these two effects.

Discussion

Our calculations raise three important and interrelated ques-

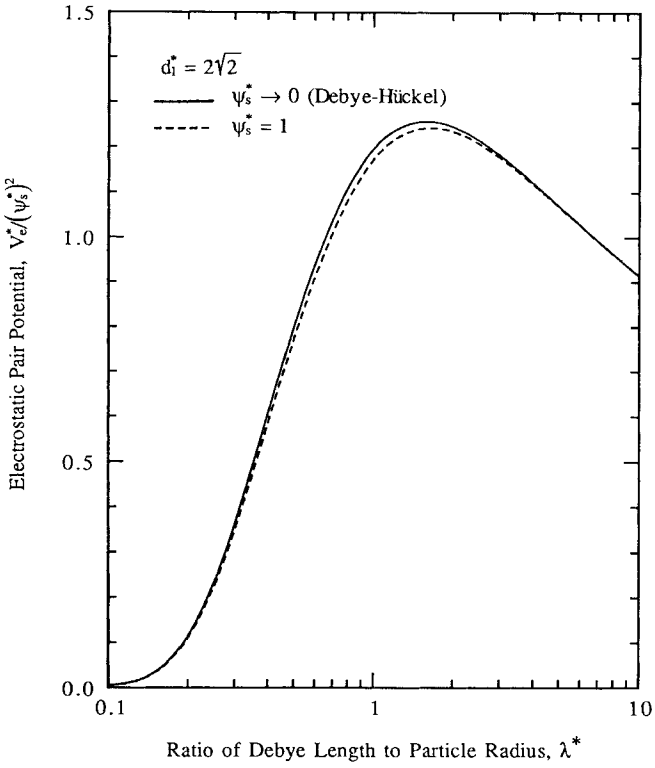

Figure 15. Dimensionless pair potential, $V_e^*/(\psi_s^*)^2$, vs. ratio of Debye length to particle radius, λ^*, for small ($\psi_s^* \to 0$) and intermediate ($\psi_s^* = 1$) fixed surface potentials between disks at a dimensionless separation, d_1^*, of $2\sqrt{2}$.

This distance corresponds to the separation between nearest neighbors in a hexagonal array at half of closest packing.

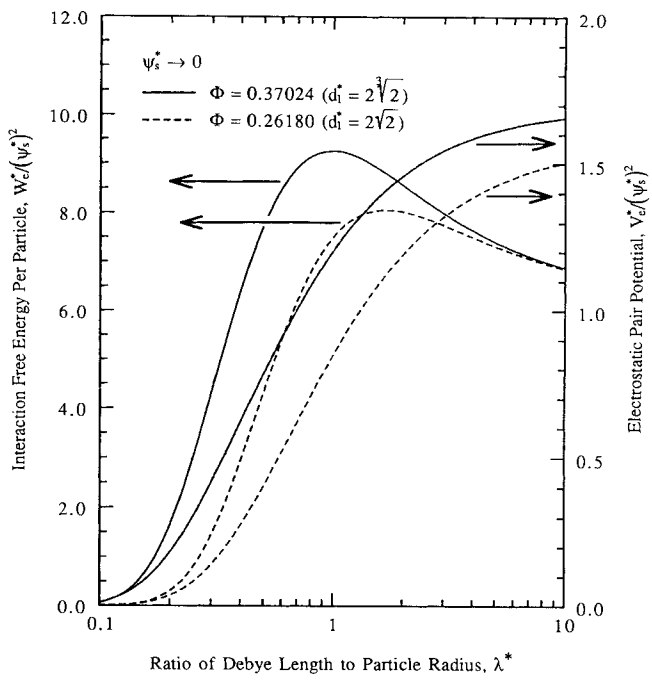

Figure 16. Dimensionless free energy per particle, $W_e^*/(\psi_s^*)^2$, for cell model 1 and dimensionless pair potential, $V_e^*/(\psi_s^*)^2$, versus ratio of Debye length to particle radius, λ^*, for spherical particles at fixed surface potential in the Debye-Hückel limit $\psi_s^* \to 0$.

Curves for the cell model correspond to 1/2 and $1/2\sqrt{2}$ of closest packing, while the pair potential curves are for dimensionless separations, d_1^*, between nearest neighbors in a face-centered cubic lattice at these volume fractions.

tions about electrostatic interactions in colloidal suspensions. First, why does W_e^* as a function of λ^* display a maximum for constant ψ_s^*? Second, since our study has been restricted to a two-dimensional model, what implications does it have for suspensions of spherical particles? Finally, if the sum of pair potentials is indeed poor over so large a range of conditions, how may double-layer free energies be approximated in concentrated suspensions? In this section, we address the first two of these issues in turn. Possible construction of effective pair and multiparticle potentials is discussed extensively in the thesis of Reiner (1991).

We were initially quite surprised to discover the nonmonotonic dependence of W_e^* on the Debye length for the array and the cell models in the calculations for fixed surface potential represented in Figure 12. This behavior is in stark contrast to that of the free energy calculated as the sum of pair potentials, which remains an increasing function of λ^*. Examination of the actual pair potentials V_e^* for $\psi_s^* \to 0$ and $\psi_s^* = 1$ shown in Figure 15 reveals, however, that these also are not monotonic functions of the Debye length. This behavior is remarkable, since a basic heuristic of the theory of colloidal stability asserts that the strength of the electrostatic repulsion between charged particles increases as the concentration of screening ions in the electrolyte is decreased, and, hence, the Debye length is increased. We next questioned whether the maximum in W_e^* is a purely two-dimensional effect. Given the similarity between our results at low and intermediate potentials, we considered it satisfactory to examine only the $\psi_s^* \to 0$ limit in three dimensions. It is straightforward to obtain the analogue to Eq. 32 for a spherical cell. The dimensionless free energy per particle may be found to be:

$$W_e^*\text{cell} \equiv \frac{W_e^{\text{cell}}}{aD\epsilon_0}\left(\frac{e}{kT}\right)^2 = \frac{4\pi\psi_s^{*2}(\lambda^* + r_{\max}^*)}{\lambda^*\{\lambda^* + r_{\max}^* - (\lambda^* - r_{\max}^*)\exp[2(r_{\max}^* - 1)/\lambda^*]\}} \quad (39)$$

where all quantities are defined as for the cylindrical cell model. Similarly, the nondimensionalized Debye-Hückel pair potential between two spherical particles at constant potential separated by a distance d_1 may be obtained by extremizing the expression:

$$V_e^* \equiv \frac{V_e}{aD\epsilon_0}\left(\frac{e}{kT}\right)^2 = 4\pi\psi_s^{*2}\left(\frac{\lambda^*+1}{\lambda^*}\right) - 2\pi b^* \int_0^{\eta_0} d\eta \int_0^{\pi} \frac{d\xi \sin(\xi)}{\cosh(\eta) - \cos(\xi)} \left\{\left[\left(\frac{\partial\psi^*}{\partial\xi}\right)^2 + \left(\frac{\partial\psi^*}{\partial\eta}\right)^2\right] + \left(\frac{b^*}{\cosh(\eta) - \cos(\xi)}\right)^2 \left(\frac{\psi^*}{\lambda^*}\right)^2\right\} \quad (40)$$

where $\eta_0(d_1^*)$ is the same function as for two disks.

We modified our finite element programs to permit the calculation implied by Eq. 40; this required minor changes to only a few lines of code. Computational characteristics and accuracy were essentially identical to those described above for cylindrical geometry. We chose to examine the Debye length dependence of Eqs. 39 and 40 over the same range of values of λ^* considered previously. Interparticle distances were selected to characterize a face-centered cubic lattice at 1/2 and $1/2\sqrt{2}$ of closest packing, corresponding to $d_1^* = 2\sqrt[3]{2}$ and $2\sqrt{2}$. These values were chosen to represent the same fraction of closest packing and the same nearest neighbor distance, respectively, as in our two-dimensional work. For this lattice, the volume fraction and interparticle separation are related by:

$$\Phi = \frac{4\pi\sqrt{2}}{3(d_1^*)^3}. \tag{41}$$

The outer boundary of the cell model was fixed at:

$$r_{\max}^* = r_v^* = \Phi^{-1/3} = d_1^* \left(\frac{3}{4\pi\sqrt{2}}\right)^{1/3}, \tag{42}$$

to yield the correct volume fraction.

The results of these calculations are shown in Figure 16, in which the axis scale for the dependent variables is chosen so that the pair and cell curves would coincide if only nearest neighbors in the lattice contributed to the pair sum and if the cell model represented precisely the geometry of the face-centered cubic lattice's rhombic dodecahedral unit cell. The behavior of the cell model is qualitatively similar to that appearing in Figure 12, but the maxima are somewhat less sharp, becoming more prominent as the volume fraction increases. Fascinatingly, the pair potentials display purely monotonic behavior, unlike those shown in Figure 15. We infer that the appearance of maxima in three dimensions is a strongly concentration-dependent phenomenon.

To rationalize these observations, it is helpful to recall the first equality in Eq. 29 which implies that for constant surface potential conditions in the DH limit:

$$W_e^* \text{cell} = \frac{-1}{2} \int_S d\underline{r}^{s*} \{q_s^*(\underline{r}^{s*}) - q_s^*(\underline{r}^{s*,\infty})\} \psi_s^*(\underline{r}^{s*}), \tag{43}$$

where the superscript $^\infty$ again represents an isolated particle. At small λ^*, the surface charge density of a single particle is large, since the potential decreases rapidly with distance from the surface. However, particles more than a Debye length apart interact weakly, so that the change in q_s^* resulting from the approach of one or more particles is correspondingly small. In this regime, the interaction free energy of a fixed arrangement of particles increases strongly as λ^* is raised. In contrast, at large Debye lengths the potential decays slowly away from the surface, and the imposition of an additional symmetry condition at $r_{\max}^*$ can do little to reduce further this decline. For λ^* much greater than $r_{\max}^* - 1$, this effect dominates the interaction between closely-packed particle configurations. If typical separations are of the order of a few particle radii, a maximum in W_e^* appears between these two limiting regimes. Pairs of cylinders display a similar phenomenon, since interactions between nearby surfaces contribute primarily to the free energy. The nearly touching portions of two spheres, however, comprise a smaller portion of W_e^* than for cylinders because of the greater curvature of the former. As a result, the free energy remains monotonic.

The influence of curvature on the monotonicity of the interaction free energy as a function of λ may be observed further from the behavior of W_e for a regular array of flat plates at fixed surface potential. Here, the lattice, cell, and pair geometries are identical, so that the value of W_e per plate is exactly equal to V_e for nearest neighbors. If the pair surface-surface separation is denoted by h, then the pair potential in the DH approximation is given by (Verwey and Overbeek, 1948):

$$\frac{h}{2D\epsilon_0(\psi_s)^2} V_e = \left(\frac{h}{2\lambda}\right)\left[1 - \tanh\left(\frac{h}{2\lambda}\right)\right]. \tag{44}$$

This particular nondimensionalization of V_e is quite revealing, since it displays the universality of the Debye length dependence of the free energy. It may thus be shown that W_e ($= V_e$) for flat plates possesses a maximum for all h, which occurs at the value of $2\lambda/h$ at which the first derivative of Eq. 44 with respect to λ vanishes. This condition is satisfied at $2\lambda/h \approx 1.564376588\ldots$

Although the nonmonotonic dependence of W_e on the Debye length weakens drastically in two and three dimensions as interparticle separations are increased, it is possible to demonstrate that the cell model free energies (Eqs. 33 and 42) retain a maximum as $r_{\max}^*$ approaches infinity; details of this analysis are presented elsewhere (Reiner, 1991). The appearance of a maximum in the interaction free energy for planar surfaces has been discussed previously by Verwey and Overbeek (1948). We believe, however, that our calculations are the first to reveal this effect in higher dimensions.

Because of the marked disparity between the qualitative behavior of the pair potentials and cell model free energies in three dimensions, it is incumbent to question the applicability of our conclusions about these approximations for cylinders to systems of spherical particles. The high symmetry of crystal lattices in three dimensions suggests that ordered configurations of spheres can be treated accurately by the cell approach. For example, the shapes of the rhombic dodecahedral and truncated octahedral unit cells that correspond respectively to the face-centered and body-centered cubic structures observed in concentrated monodisperse suspensions are well-approximated by spheres of the same volume. Indeed, it was in the context of a study of the somewhat similar problem to the one we have examined of calculating free electron wave functions and lattice energies in metals of precisely these structures that the replacement of intricate lattice geometry by a simpler spherical cell of the same volume was first suggested (Wigner and Seitz, 1933). Conversely, the implications of greater dimensionality for the pair approximation are negative, but perhaps less definitive. The higher coordination number of dense systems of spherical particles implies that their multiple double-layer overlap is even more significant than that for configurations of cylinders. However, the electrostatic potential decays slightly more rapidly with distance from a spherical surface, in comparison to a cylindrical surface. Accordingly, the effect of multiple double-layer overlap among spherical particles may

be partially reduced, particularly at small volume fractions. Precise understanding of these issues must await more careful calculations in three dimensions, since assessment of their importance is made difficult by the complexity of particle packings. We assert that the results for the cell model shown in Figure 16 are more likely to be representative of interaction free energies in concentrated suspensions of spheres than those obtained from the corresponding pair computations.

Conclusions

We have computed accurate numerical values of the electrostatic interaction free energy for a hexagonal model of a concentrated suspension of charged colloidal particles by applying an efficient finite element technique to the variational theory for double-layer interactions derived by Reiner and Radke (1990). Our results range over two orders of magnitude of fixed surface charges and potentials and over a similar range of Debye lengths for particle volume fractions up to 96% of closest packing. These values of W_e^* were compared to those approximated by summing calculated pair interactions over 11 shells of nearest neighbors and by replacing the hexagonal unit cell boundary surrounding a central particle by a cylinder enclosing the same volume (model 1) or with a radius equal to half the distance of closest approach of the particle's nearest neighbors (model 2). In particular, analytical results for the interaction free energy in the Debye-Hückel approximation were derived for the cylindrical cell model and for its spherical analogue.

The pair approximation fared poorly over most of the conditions which we considered. Only for very small volume fractions (or, more generally, Debye lengths much shorter than typical surface-surface separations) did it yield quantitatively accurate results. The first implementation of the cell model performed much better, erring from the exact hexagonal values of W_e^* at very short Debye lengths, where detailed aspects of configurational geometry strongly influence the free energy, whereas the second remained qualitatively, but not quantitatively, correct for all sets of parameters. We observe little systematic influence of surface charge density or potential on the accuracy of any of the approximations, but a fortuitous cancellation of errors causes the pair sum to yield precise numerical results at intermediate surface charges.

We have observed a particularly interesting phenomenon as the ionic strength of the electrolyte surrounding the suspended particles is altered by varying the Debye length. The interaction free energy exhibits a maximum as a function of λ^* in both the hexagonal and cell calculations for constant surface potential conditions. This behavior is also observed in the pair potentials, but the corresponding sums of these two-particle interactions remain monotonic. In three dimensions, the spherical cell model free energy displays a similar maximum, while pair potentials remain strictly increasing functions of the Debye length. Although the nonmonotonic dependence of W_e on λ for pairs of flat plates with identical surface potentials was discussed long ago by Verwey and Overbeek (1948), to our knowledge our results demonstrate this behavior in cylindrical and spherical geometries for the first time. We conclude that there are significant concentration-dependent effects in colloidal dispersions which merit further study, both theoretically and experimentally.

Our calculations raise substantial concerns about the applicability of pair-potential based theories to highly concentrated suspensions. Although the use of such approaches has been almost ubiquitous thus far, it is clear that a more critical evaluation of their suitability and a thorough investigation of their alternatives are now necessary.

Acknowledgment

Portions of this work were originally presented at the Gordon Conference on Ceramics in Plymouth, NH (July–August, 1985) and the Summer National Meeting of the American Institute of Chemical Engineers in Seattle, WA (August, 1985). We acknowledge partial support from the U.S. Department of Energy under Grant No. DE-AC03-76SF00098 to the Lawrence Berkeley Laboratories of the University of California. We also thank the Academic Computing Services of the University of California for a grant of computer time on the Berkeley Cray XMP-14.

Notation

a = particle radius, m
b = parameter used in definition of bipolar coordinates, m
b^* = dimensionless form of b, defined by $b^* \equiv b/a$
C_i^0 = bulk concentration of ion i, mol/m^3
d = interparticle center-center separation, m
d_τ = center-center distance between a central particle and a particle in neighbor shell τ, m
d_1 = nearest neighbor distance, m
d_1^* = dimensionless value of d_1, defined by $d_1^* \equiv d_1/a$
$D(\underset{\sim}{r})$ = local value of the electrolyte dielectric constant
e = unit charge, C
$g_i(\underset{\sim}{r})$ = singlet distribution of ion i at $\underset{\sim}{r}$ within the double layer
h = interparticle surface-surface separation, m
I_0, I_1 = modified Bessel functions of the first kind
i = index for summation over ions; ion valence
$\imath$ = square root of -1
j = index for summation over elements in the basis ϕ
k = Boltzmann's constant, J/K
K_0, K_1 = modified Bessel functions of the second kind
m = total number of colloidal particles
n = number of ionic species present in the electrolyte
$\underset{\sim}{n}$ = unit vector normal to a particle surface, directed *into* the electrolyte
N_c = coordination number of a particle configuration
N_i = total number of ions of species i within the double layer, mol
p = total number of parameters α_j in the expansion (Eq. 38)
$q_s(\underset{\sim}{r}^s)$ = charge density at particle surface, C/m^2
q_s^* = dimensionless value of q_s, defined by $q_s^* \equiv q_s ea/D\epsilon_0 kT$
r = radial coordinate for cylindrical and spherical cell models, m
$\underset{\sim}{r}$ = position in the double layer, m
$\underset{\sim}{r}^s$ = position on a particle surface or system boundary, m
$\underset{\sim}{r}^{s*}$ = dimensionless surface coordinate
r^* = dimensionless form of r, defined by $r^* \equiv r/a$
$\underset{\sim}{r}^*$ = dimensionless position in the double layer
r_d^* = dimensionless location of the outer boundary of the "nearest neighbor" symmetric cell model (cell model 2).
$r_{\max}^*$ = dimensionless location of the outer boundary of the symmetric cell model
r_v^* = dimensionless location of the outer boundary of the volume fraction equivalent cell model (cell model 1)
S = surface area of the particles and enclosing boundary, m^2
S = point set comprising the particle surfaces and system boundary
T = absolute temperature, K
V = volume of electrolyte enclosed in system, m^3
V_a = van der Waals potential between two colloidal particles, J
V_b = short range repulsive potential between two colloidal particles, J

V_e = configurational electrostatic interaction free energy between two colloidal particles (per unit length in two dimensions), J or J/m

V_e^* = dimensionless value of V_e, defined by $V_e^* \equiv (V_e/D\epsilon_0)(e/kT)^2$ in two dimensions and $V_e^* \equiv (V_e/aD\epsilon_0)(e/kT)^2$ in three dimensions

V_t = total interaction potential between two colloidal particles $\equiv V_e + V_a + V_b$, J

V = point set comprising the volume of electrolyte in the system

W_e = interaction free energy of a configuration of colloidal particles (per unit length in two dimensions), J or J/m

W_e^* = dimensionless value of W_e, defined by $W_e^* \equiv (W_e/D\epsilon_0)(e/kT)^2$ in two dimensions and $W_e^* \equiv (W_e/aD\epsilon_0)(e/kT)^2$ in three dimensions

x = Cartesian coordinate, m

y = Cartesian coordinate, m

z = complex form of Cartesian coordinates, $z = x + iy$, m

z' = complex form of bipolar coordinates, $z' = \xi + i\eta$

z_i = valence of ion i

Z_τ = coordination number of shell τ in a regular array of particles

Greek letters

$\underset{\sim}{\alpha}$ = vector of parameters α_j

α_j = variational parameter multiplying the basis function ϕ_j in the expansion, Eq. 38

δ = variational operator

$\delta\psi(\underset{\sim}{r})$ = infinitesimal variation of $\psi(\underset{\sim}{r})$

ϵ_0 = dielectric permittivity of free space, C/V•m

ζ = transformation of the radial coordinate r^* for the symmetric cell model, defined by Eq. 35

ζ_{max} = value of ζ corresponding to r^*_{max}

η = bipolar coordinate defined by Eq. 18

η_0 = location of a particle surface in bipolar coordinate system

ϑ = smallness parameter for errors in $\psi(\underset{\sim}{r})$

λ = Debye length, defined by Eq. 5, m

λ^* = dimensionless Debye length, defined by $\lambda^* \equiv \lambda/a$

μ_i = chemical potential of ion i, J/mol

ν, ν' = indices for summation over colloidal particles

ξ = bipolar coordinate, defined by Eq. 18

$\xi_0(\eta)$ = bipolar coordinate parameterization of the hexagonal cell symmetry line at an angle of $\pi/6$ radians with respect to the x-axis

$\Pi_{osm}(\underset{\sim}{r})$ = osmotic pressure due to ions at $\underset{\sim}{r}$ within the double layer, J/m^3

Π^0_{osm} = bulk value of Π_{osm}, J/m^3

$\rho_e(\underset{\sim}{r})$ = charge density at $\underset{\sim}{r}$, C/m^3

τ = index for summation over shells of neighbors in a regular array of particles

Φ = particle volume (or area) fraction

ϕ = approximate basis for ψ in V

ϕ_j = jth member of the basis ϕ

$\psi(\underset{\sim}{r})$ = electrostatic potential at $\underset{\sim}{r}$ within the double layer, V

ψ^* = dimensionless potential, defined by $\psi^* \equiv e\psi/kT$

$\psi_s(\underset{\sim}{r}^s)$ = value of the electrostatic potential at surface coordinate $\underset{\sim}{r}^s$, V

ψ_s^* = dimensionless surface potential, defined by $\psi_s^* \equiv e\psi_s/kT$

Ω_e = electrostatic grand free energy functional, J (J/m in two dimensions)

Ω_e^* = dimensionless value of Ω_e, defined by $\Omega_e^* \equiv (\Omega_e/D\epsilon_0)(e/kT)^2$ in two dimensions and $\Omega_e^* \equiv (\Omega_e/aD\epsilon_0)(e/kT)^2$ in three dimensions

$\omega_s(\underset{\sim}{r}^s)$ = surface free energy density, J/m^2

Superscripts

cell = free energy calculated for the symmetric cell model

pair = interactions between pairs of particles

pair sum = free energy value approximated as the sum of pair potentials

particle = free energy value per particle in a regular array

subcell = free energy of one of the symmetric regions surrounding a particle in a regular array

* = dimensionless quantity

$^\infty$ = isolated particle

Others

$\underset{\sim}{\nabla}$ = gradient operator, m^{-1}

$\underset{\sim}{\nabla}^*$ = dimensionless gradient operator, defined by $\underset{\sim}{\nabla}^* \equiv a\underset{\sim}{\nabla}$

$\langle\ \rangle$ = enclosed quantity averaged in the grand ensemble

Literature Cited

Ackerson, B. J., and N. A. Clark, "Shear-Induced Melting," *Phys. Rev. Lett.*, **46**, 123 (1981).

Ackerson, B. J., and N. A. Clark, "Shear-Induced Partial Translational Ordering of a Colloidal Solid," *Phys. Rev. A*, **30**, 906 (1984).

Ackerson, B. J., and P. N. Pusey, "Shear-Induced Order in Suspensions of Hard Spheres," *Phys. Rev. Lett.*, **61**, 1033 (1988).

Alexandrowicz, Z., "Calculation of the Thermodynamic Properties of Polyelectrolytes in the Presence of Salt," *J. Polym. Sci.*, **56**, 97 (1962).

Alexandrowicz, Z., and A. Katchalsky, "Colligative Properties of Polyelectrolyte Solutions in Excess of Salt," *J. Polym. Sci.*, **A1**, 3231 (1963).

Alfrey, T., P. W. Berg, and H. Morawetz, "The Counterion Distribution in Solutions of Rod-Shaped Polyelectrolytes," *J. Polym. Sci.*, **7**, 543 (1951).

Bacquet, R., and P. J. Rossky, "Ionic Atmosphere of Rodlike Polyelectrolytes. A Hypernetted Chain Study," *J. Phys. Chem.*, **88**, 2660 (1984).

Bagchi, B., and D. Thirumalai, "Freezing of a Colloidal Liquid Subject to Shear Flow," *Phys. Rev. A*, **37**, 2530 (1988).

Barclay, L., A. Harrington, and R. H. Ottewill, "The Measurement of Forces Between Particles in Disperse Systems," *Kolloid-Zeitschrift und Zeitschrift für Polymere*, **250**, 655 (1972).

Barringer, E., and H. K. Bowen, "Formation, Packing, and Sintering of Monodisperse TiO_2 Powders," *Commun. of Amer. Ceramic Soc.*, **65**, C199 (1983).

Bell, G. M., and S. Levine, "Statistical Thermodynamics of Concentrated Colloidal Solutions: 1. Free Energy of Electrical Double Layers," *Trans. Faraday Soc.*, **53**, 143 (1957).

Bell, G. M., S. Levine, and L. N. McCartney, "Approximate Methods of Determining the Double-Layer Free Energy of Interaction between Two Charged Colloidal Spheres," *J. Coll. Int. Sci.*, **33**, 335 (1970).

Bell, G. M., and G. C. Peterson, "Calculation of the Electric Double-Layer Force Between Unlike Spheres," *J. Coll. Int. Sci.*, **41**, 542 (1972).

Bernal, J. D., and I. Fankuchen, "X-Ray and Crystallographic Studies of Plant Virus Preparations: I. Introduction and Preparation of Specimens, II. Modes of Aggregation of the Virus Particles," *J. Gen. Physiol.*, **25**, 111 (1941).

Bertsekas, D. P., *Notes on Nonlinear Programming and Discrete-Time Optimal Control*, Laboratory for Information and Decision Systems, M.I.T., Cambridge, MA (1982).

Beunen, J. A., and L. R. White, "The Order-Disorder Transition in Latex Dispersions," *Colloids and Surfaces*, **3**, 371 (1981).

Bierman, A., "An Application of the Poisson-Boltzmann Equation to Nonidentical Charged Particles," *Proc. Nat. Acad. Sci. USA*, **41**, 245 (1955a).

Bierman, A., "Electrostatic Forces Between Nonidentical Colloidal Particles," *J. Coll. Sci.*, **10**, 231 (1955b).

Blum, L., J. Hernando, and J. L. Lebowitz, "Numerical Method and General Discussion of Integral Equations for the Primitive Model of the Electric Interface," *J. Phys. Chem.*, **87**, 2825 (1983).

Bossis, G., and J. F. Brady, "Dynamic Simulation of Sheared Suspensions: I. General Method," *J. Chem. Phys.*, **60**, 5141 (1984).

Brandes, R., and D. R. Kearns, "Magnetic Ordering of DNA Liquid Crystals," *Biochemistry*, **25**, 5890 (1986).

Brenner, S. L., and D. A. McQuarrie, "A Self-consistent Calculation of the Free Energy and Electrostatic Potential for a Cylindrical Polyion," *J. Theor. Biol.*, **39**, 343 (1973a).
Brenner, S. L., and D. A. McQuarrie, "On the Theory of the Electrostatic Interaction Between Cylindrical Polyelectrolytes," *J. Coll. Int. Sci.*, **44**, 298 (1973b).
Brenner, S. L., and D. A. McQuarrie, "Force Balances in Systems of Cylindrical Polyelectrolytes," *Biophys. J.*, **13**, 301 (1973c).
Carnie, S. L., "Hypernetted-Chain Theories of the Primitive Model Double Layer, A Last Look at Binary Symmetric Electrolytes," *Mol. Phys.*, **54**, 509 (1985).
Carnie, S. L., and D. Y. C. Chan, "Ionic and Dipolar Adsorption from an Ion-Dipole Mixture, A Model for the Stern Layer," *J. Chem. Soc. Faraday Trans. II*, **78**, 695 (1982).
Carnie, S. L., D. Y. C. Chan, D. J. Mitchell, and B. W. Ninham, "The Structure of Electrolytes at Charged Surfaces: The Primitive Model," *J. Chem. Phys.*, **74**, 1472 (1981).
Carnie, S. L., G. M. Torrie, and J. P. Valleau, "Ion-Size Effects in the Primitive Model Double Layer," *Mol. Phys.*, **53**, 253 (1984).
Chan, D., T. W. Healy, and L. R. White, "Electrical Double Layer Interactions under Regulation by Surface Ionization Equilibria—Dissimilar Amphoteric Surfaces," *J. Chem. Soc. Faraday Trans. I*, **72**, 2844 (1976).
Chan, D., J. W. Perram, L. R. White, and T. W. Healy, "Regulation of Surface Potential at Amphoteric Surfaces during Particle-Particle Interaction," *J. Chem. Soc. Faraday Trans. I*, **71**, 1046 (1975).
Chapman, D. L., "A Contribution to the Theory of Electrocapillarity," *Phil. Mag.*, **25**, 475 (1913).
Chen, C. S., and S. Levine, "Double Layer Interaction Energy of a Concentrated System of Charged Parallel Colloidal Plates in Aqueous Electrolyte," *J. Chem. Soc. Faraday Trans. II*, **68**, 1497 (1972).
Clark, N. A., and B. J. Ackerson, "Observation of the Coupling of Concentration Fluctuations to Steady-State Shear Flow," *Phys. Rev. Lett.*, **44**, 1005 (1980).
Derjaguin, B., "Unterschungen Über die Reibung und Adhäsion, IV. Theorie des Anhaftens Kleiner Teilchen," *Kolloid-Zeitschrift*, **69**, 155 (1934).
Derjaguin, B., "A Theory of Interaction of Particles in Presence of Electric Double Layers and the Stability of Lyophobic Colloids and Disperse Systems," *Acta Physiochimica U.R.S.S.*, **10**, 334 (1939).
Derjaguin, B., and L. Landau, "Theory of the Stability of Strongly Charged Lyophobic Sols and of the Adhesion of Strongly Charged Particles in Solutions of Electrolytes," *Acta Physiochimica U.R.S.S.*, **14**, 633 (1941).
Dube, G. P., "Electrical Energy of Two Cylindrical Charged Particles," *Indian J. Phys.*, **17**, 189 (1943).
Einevoll, G., and P. C. Hemmer, "Spatial Distribution of Ions Around Rod-like Polyelectrolytes," *J. Chem. Phys.*, **89**, 474 (1988).
Elliott, G. F., "Force-Balances and Stability in Hexagonally-Packed Polyelectrolyte Systems," *J. Theor. Biol.*, **21**, 71 (1968).
Fixman, M., "The Poisson-Boltzmann Equation and its Application to Polyelectrolytes," *J. Chem. Phys.*, **70**, 4995 (1979).
Fuoss, R. M., A. Katchalsky, and S. Lipson, "The Potential of an Infinite Rod-Like Molecule and the Distribution of the Counter Ions," *Proc. Nat. Acad. Sci. USA*, **37**, 579 (1951).
Glendinning, A. B., and W. B. Russel, "The Electrostatic Repulsion Between Charged Spheres from Exact Solutions to the Linearized Poisson-Boltzmann Equation," *J. Coll. Int. Sci.*, **93**, 95 (1983).
Gouy, M., "Sur la Constitution de la Charge Électrique a la Surface d'un Électrolyte," *J. de Physique*, **9**, 457 (1910).
Guldbrand, L., L. G. Nilsson, and L. Nordenskiöld, "A Monte Carlo Simulation Study of Electrostatic Forces between Hexagonally Packed DNA Double Helices," *J. Chem. Phys.*, **85**, 6686 (1986).
Hachisu, S., and Y. Kobayashi, "Kirkwood-Alder Transition in Monodisperse Latexes: II. Aqueous Latexes of High Electrolyte Concentration," *J. Coll. Int. Sci.*, **46**, 470 (1974).
Hachisu, S., Y. Kobayashi, and A. Kose, "Phase Separation in Monodisperse Latexes," *J. Coll. Int. Sci.*, **42**, 342 (1973).
Hachisu, S., and S. Yoshimura, "Optical Demonstration of Crystalline Superstructures in Binary Mixtures of Latex Globules," *Nature (London)*, **283**, 188 (1980).
Hamaker, H. C., "The London-van der Waals Attraction Between Spherical Particles," *Physica*, **4**, 1058 (1937).
Happel, J., and H. Brenner, *Low Reynolds Number Hydrodynamics*, 2nd ed., Nijhoff, Dordrecht, the Netherlands (1973).
Healy, T. W., D. Chan, and L. R. White, "Colloidal Behavior of Materials With Ionizable Group Surfaces," *Pure & Appl. Chem.*, **52**, 1207 (1980).
Henderson, D., and L. Blum, "Some Exact Results and the Application of the Mean Spherical Approximation to Charged Hard Spheres near a Charged Hard Wall," *J. Chem. Phys.*, **69**, 5441 (1978).
Henderson, D., and L. Blum, "A Simple Non-iterative Method for Calculating the Potential of an Electric Double Layer," *J. Electroanal. Chem.*, **111**, 217 (1980).
Henderson, D., and L. Blum, "The Application of the Generalized Mean Spherical Approximation to the Theory of the Diffuse Double Layer," *Can. J. Chem.*, **59**, 1906 (1981).
Henderson, D., L. Blum, and W. R. Smith, "Application of the Hypernetted-Chain Approximation to the Electric Double Layer at a Charged Planar Interface," *Chem. Phys. Lett.*, **63**, 381 (1979).
Hiltner, P. A., and I. M. Krieger, "Diffraction of Light by Ordered Suspensions," *J. Phys. Chem.*, **73**, 2386 (1969).
Hoffman, R. L., "Discontinuous and Dilatant Viscosity Behavior in Concentrated Suspensions: I. Observation of a Flow Instability," *Trans. Soc. Rheo.*, **16**, 155 (1972).
Hoffman, R. L., "Discontinuous and Dilatant Viscosity Behavior in Concentrated Suspensions: II. Theory and Experimental Tests," *J. Coll. Int. Sci.*, **46**, 491 (1974).
Hoffman, R. L., "Discontinuous and Dilatant Viscosity Behavior in Concentrated Suspensions: III. Necessary Conditions for Their Occurrence in Viscometric Flows," *Adv. Coll. Int. Sci.*, **17**, 161 (1982).
Hogg, R., T. W. Healy, and D. W. Fuerstenau, "Mutual Coagulation of Colloidal Dispersions," *Trans. Faraday Soc.*, **62**, 1638 (1966).
Honig, E. P., and P. M. Mul, "Tables and Equations of the Diffuse Double Layer Repulsion at Constant Potential and Constant Charge," *J. Coll. Int. Sci.*, **36**, 258 (1971).
Hoskin, N. E., and S. Levine, "The Interaction of Two Identical Spherical Colloidal Particles: II. The Free Energy," *Phil. Trans. Roy. Soc.*, **A248**, 449 (1956).
Kar, G., S. Chander, and T. S. Mika, "The Potential Energy of Interaction Between Dissimilar Electrical Double Layers," *J. Coll. Int. Sci.*, **44**, 347 (1973).
Kose, A., and S. Hachisu, "Kirkwood-Alder Transition in Monodisperse Latexes: I. Nonaqueous Systems," *J. Coll. Int. Sci.*, **46**, 460 (1974).
Kose, A., M. Ozaki, K. Takano, Y. Kobayashi, and S. Hachisu, "Direct Observation of Ordered Latex Suspension by Metallurgical Microscope," *J. Coll. Int. Sci.*, **44**, 330 (1973).
Le Bret, M., and B. H. Zimm, "Monte Carlo Determination of the Distribution of Ions About a Cylindrical Polyelectrolyte," *Biopolymers*, **23**, 271 (1984).
Levine, S., "Problem of the Sedimentation Equilibrium in Colloidal Suspensions," *Proc. Roy. Soc.*, **A146**, 597 (1934).
Levine, S., "Problems of Stability in Hydrophobic Colloidal Solutions: I. On the Interaction of Two Colloidal Metallic Particles—General Discussion and Applications," *Proc. Roy. Soc.*, **A170**, 145 (1939a).
Levine, S., "Problems of Stability in Hydrophobic Colloidal Solutions: II. On the Interaction of Two Colloidal Metallic Particles—Mathematical Theory," *Proc. Roy. Soc.*, **A170**, 165 (1939b).
Levine, S., "On the Interaction of Two Colloidal Particles, Using the Complete Debye-Hückel Equation," *J. Chem. Phys.*, **7**, 831 (1939c).
Lifson, S., and A. Katchalsky, "The Electrostatic Free Energy of Polyelectrolyte Solutions: II. Fully Stretched Macromolecules," *J. Polym. Sci.*, **13**, 43 (1954).
Linse, P., and B. Jönsson, "A Monte Carlo Study of the Electrostatic Interaction Between Highly Charged Aggregates: A Test of the Cell Model Applied to Micellar Systems," *J. Chem. Phys.*, **78**, 3167 (1983).
Lozada-Cassou, M., and D. Henderson, "Application of the Hypernetted Chain Approximation to the Electrical Double Layer: Comparison with Monte Carlo Results for 2:1 and 1:2 Salts," *J. Phys. Chem.*, **87**, 2821 (1983).
Lozada-Cassou, M., R. Saavedra-Barrera, and D. Henderson, "The Application of the Hypernetted Chain Approximation to the Electrical Double Layer: Comparison with Monte Carlo Results for Symmetric Salts," *J. Chem. Phys.*, **77**, 5150 (1982).
Luck, W., M. Klier, and H. Wesslau, "Über Bragg-Reflexe mit Sicht-

barem Licht an Monodispersen Kunststofflatices: I," *Ber. Bunsenges. Phys. Chem.*, **67**, 75 (1963).
Marčelja, S., D. J. Mitchell, and B. W. Ninham, "Phase Transitions in Aqueous Suspensions of Spherical Colloid Particles," *Chem. Phys. Lett.*, **43**, 353 (1976).
McCartney, L. N., and S. Levine, "An Improvement on Derjaguin's Expression at Small Potentials for the Double Layer Interaction Energy of Two Spherical Colloidal Particles," *J. Coll. Int. Sci.*, **30**, 345 (1969).
Millman, B. M., T. C. Irving, B. G. Nickel, and M. E. Loosley-Millman, "Interrod Forces in Aqueous Gels of Tobacco Mosaic Virus," *Biophys. J.*, **45**, 551 (1984).
Millman, B. M., and B. G. Nickel, "Electrostatic Forces in Muscle and Cylindrical Gel Systems," *Biophys. J.*, **32**, 49 (1980).
Mills, P., C. F. Anderson, and M. T. Record, "Monte Carlo Studies of Counterion-DNA Interactions. Comparison of the Radial Distribution of Counterions with Predictions of Other Polyelectrolyte Theories," *J. Phys. Chem.*, **89**, 3984 (1985).
Mori, M., *The Finite Element Method and Its Applications*, Macmillan, New York (1986).
Morse, P. M., and H. Feshbach, *Methods of Theoretical Physics*, Vol. 2, McGraw-Hill, New York (1953).
Murthy, C. S., R. J. Bacquet, and P. J. Rossky, "Ionic Distributions Near Polyelectrolytes. A Comparison of Theoretical Approaches," *J. Phys. Chem.*, **89**, 701 (1985).
Ninham, B. W., and V. A. Parsegian, "Electrostatic Potential Between Surfaces Bearing Ionizable Groups in Ionic Equilibrium with Physiologic Saline Solution," *J. Theor. Biol.*, **31**, 405 (1971).
Ohshima, H., D. Y. C. Chan, T. W. Healy, and L. R. White, "Improvement on the Hogg-Healy-Fuerstenau Formulas for the Interaction of Dissimilar Double Layers: II. Curvature Correction to the Formula for the Interaction of Spheres," *J. Coll. Int. Sci.*, **92**, 232 (1983).
Ohshima, H., T. W. Healy, and L. R. White, "Improvement on the Hogg-Healy-Fuerstenau Formulas for the Interaction of Dissimilar Double Layers: I. Second and Third Approximations for Moderate Potentials," *J. Coll. Int. Sci.*, **89**, 484 (1982).
Ohtsuki, T., A. Kishimoto, S. Mitaku, and K. Okano, "Studies of Ordered Monodisperse Latexes. IV. Mechanism of Ordering," *Jap. J. Appl. Phys.*, **20**, 509 (1981).
Parsegian, V. A., "Theory of Liquid-Crystal Phase Transitions in Lipid + Water Systems," *Trans. Faraday Soc.*, **62**, 848 (1966).
Press, W. H., B. P. Flannery, S. A. Teukolsky, and W. T. Vetterling, *Numerical Recipes, The Art of Scientific Computing*, Cambridge University Press, Cambridge (1986).
Rau, D. C., B. Lee, and V. A. Parsegian, "Measurement of the Repulsive Force Between Polyelectrolyte Molecules in Ionic Solution: Hydration Forces Between Parallel DNA Double Helices," *Proc. Nat. Acad. Sci. USA*, **81**, 2621 (1984).
Reiner, E. S., "Equilibrium Theory of Concentrated Colloidal Suspensions," PhD Diss., University of California, Berkeley (1991).
Reiner, E. S., and C. J. Radke, "A Variational Approach to the Electrostatic Free Energy in Charged Colloidal Suspensions: General Theory for Open Systems," *J. Chem. Soc. Faraday Trans.*, **86**, 3901 (1990).
Shih, W.-H., and D. Stroud, "Theoretical Study of the Freezing of Polystyrene Sphere Suspensions," *J. Chem. Phys.*, **79**, 6254 (1983).
Snook, I., and W. van Megen, "Prediction of Ordered and Disordered States in Colloidal Dispersions," *J. Chem. Soc. Faraday Trans. II*, **72**, 216 (1976).
Snook, I., and W. van Megen, "Finite Ion Size Effects in the Electrical Double Layer—A Monte Carlo Study," *J. Chem. Phys.*, **75**, 4104 (1981).
Sparnaay, M. J., "The Interaction between Two Cylinder Shaped Colloidal Particles," *Recl. Trav. Chim. Pays-Bas*, **78**, 680 (1959).
Strang, G., and G. J. Fix, *An Analysis of the Finite Element Method*, Prentice-Hall, Englewood Cliffs, NJ (1973).
Takano, K., and S. Hachisu, "Simulation Study of Equation of State of Simple Liquid by the Use of Monodisperse Latex," *J. Phys. Soc. Japan*, **42**, 1775 (1977).
Takano, K. and S. Hachisu, "Spectroscopic Study of Monodisperse Latex: I. Short-Range Order in Monodisperse Latex," *J. Coll. Int. Sci.*, **66**, 124 (1978a).
Takano, K., and S. Hachisu, "Spectroscopic Study of Monodisperse Latex: II. Phase Diagram of Monodisperse Latex," *J. Coll. Int. Sci.*, **66**, 130 (1978b).
Tiddy, G. J. T., "Surfactant-Water Liquid Crystal Phases," *Phys. Rep.*, **57**, 1 (1980).
Torrie, G. M., and J. P. Valleau, "Electrical Double Layers. I. Monte Carlo Study of a Uniformly Charged Surface," *J. Chem. Phys.*, **73**, 5807 (1980).
Usui, S., "Interaction of Electrical Double Layers at Constant Surface Charge," *J. Coll. Int. Sci.*, **44**, 107 (1973).
van Megen, W., and I. Snook, "Statistical Mechanical Approaches to Phase Transitions in Hydrophobic Colloids: I. Effects of Electrolyte Concentration," *J. Coll. Int. Sci.*, **57**, 40 (1976a).
van Megen, W., and I. Snook, "Statistical Mechanical Approaches to Phase Transitions in Hydrophobic Colloids: II. Effects of Particle Size," *J. Coll. Int. Sci.*, **57**, 47 (1976b).
van Megen, W., and I. Snook, "Statistical Mechanical Approach to Phase Transitions in Colloids," *Disc. Faraday Soc.*, **65**, 92 (1978).
van Megen, W., and I. Snook, "The Grand Canonical Ensemble Monte Carlo Method Applied to the Electrical Double Layer," *J. Chem. Phys.*, **73**, 4656 (1980).
Verwey, E. J. W., and J. Th. G. Overbeek, *Theory of the Stability of Lyophobic Colloids*, Elsevier, Amsterdam (1948).
Vlachy, V., and A. D. J. Haymet, "A Grand Canonical Monte Carlo Simulation Study of Polyelectrolyte Solutions," *J. Chem. Phys.*, **84**, 5874 (1986).
Wadati, M., and M. Toda, "An Evidence for the Existence of Kirkwood-Alder Transition," *J. Phys. Soc. Japan*, **32**, 1147 (1972).
Wennerström, H., and B. Lindman, "Micelles: Physical Chemistry of Surfactant Association," *Phys. Rep.*, **52**, 1 (1979).
Wigner, E., and F. Seitz, "On the Constitution of Metallic Sodium," *Phys. Rev.*, **43**, 804 (1933).
Williams, R., and R. S. Crandall, "The Structure of Crystallized Suspensions of Polystyrene Spheres," *Phys. Lett.*, **48A**, 225 (1974).
Williams, R., R. S. Crandall, and P. J. Wojtowicz, "Melting of Crystalline Suspensions of Polystyrene Spheres," *Phys. Rev. Lett.*, **37**, 348 (1976).
Winsor, P. A., "Binary and Multicomponent Solutions of Amphiphilic Compounds. Solubilization and the Formation, Structure, and Theoretical Significance of Liquid Crystalline Solutions," *Chem. Rev.*, **68**, 1 (1968).
Wolfe, M. A., *Numerical Methods for Unconstrained Optimization, an Introduction*, Van Nostrand Reinhold, New York (1978).

Manuscript received Aug. 23, 1990, and revision received Apr. 22, 1991.